bioRxiv preprint doi: https://doi.org/10.1101/579938; this version posted June 29, 2020. The copyright holder for this preprint (which was not certified by peer review) is the author/funder. All rights reserved. No reuse allowed without permission.

Dynamic changes in large-scale functional connectivity predict performance in a multisensory task

Karl J. Hollensteiner[1], Edgar Galindo-Leon[1], Florian Pieper[1], Gerhard Engler[1], Guido Nolte[1], Andreas K. Engel[1]

[1] Department of Neurophysiology and Pathophysiology, University Medical Center Hamburg-Eppendorf, 20246 Hamburg, Germany

Correspondence should be addressed to:
Karl J. Hollensteiner, Department of Neurophysiology and Pathophysiology, University Medical Center Hamburg-Eppendorf, 20246 Hamburg, Germany. Email: k.hollensteiner@uke.de

Abbreviated title: Functional connectivity predicts performance in a multisensory task

Key words: auditory cortex, electrocorticogram, ferret, phase coupling, visual cortex

Number of figures: 8

Number of words: Abstract (188), Introduction (720), Materials and Methods (2009), Results (2567), Discussion (2187).

bioRxiv preprint doi: https://doi.org/10.1101/579938; this version posted June 29, 2020. The copyright holder for this preprint (which was not certified by peer review) is the author/funder. All rights reserved. No reuse allowed without permission.

Abstract

Complex and variable behavior requires fast changes of functional connectivity in large-scale cortical networks. Here, we report on the cortical dynamics of functional coupling across visual, auditory and parietal areas during a lateralized detection task in the ferret. We hypothesized that fluctuations in coupling, indicative of dynamic variations in the network state, might predict the animals' performance. While power for hit and miss trials showed significant differences only around stimulus and response onset, phase coupling already differed before stimulus onset. Principal component analysis of directed coupling at the single-trial level during this period revealed subnetworks that most strongly related to behavior. While higher global phase coupling of visual and auditory regions to parietal cortex was predictive of task performance, a second component showed that a reduction in coupling between subnetworks of sensory modalities was also necessary, probably to allow a better detection of the unimodal signals. Furthermore, we observed that long-range coupling became more predominant during the task period compared to the pre-stimulus baseline. Taken together, these results suggest that fluctuations in the network state, particular with respect to long-range connectivity, are key determinants of the animals' behavior.

bioRxiv preprint doi: https://doi.org/10.1101/579938; this version posted June 29, 2020. The copyright holder for this preprint (which was not certified by peer review) is the author/funder. All rights reserved. No reuse allowed without permission.

Introduction

The brain continuously integrates information from different sensory systems enhancing its ability to filter noisy signals, to construct coherent percepts and guide appropriate actions (Stein and Meredith, 1993; Alais et al., 2010; Green and Angelaki, 2010; van Atteveldt et al., 2014). Such processes require the flexible and coordinated orchestration of distributed neuronal populations within and across brain areas (Singer and Gray, 1995; Engel et al., 2001; Fries, 2005; Senkowski et al., 2008; Siegel et al., 2012). Numerous studies have shown that this orchestration relies mostly on three modes of intrinsically generated coupling: synchronization of neural phase, the correlation of amplitude envelopes and the correlation between phase and amplitude (Raichle, 2010; Canolty and Knight, 2010; Siegel et al., 2012; Engel et al., 2013; Galindo-Leon et al., 2019). In addition, these coupling modes operate in multiple frequency bands and scales, mediating different cognitive functions (Buzsaki, 2006; Jensen and Mazaheri, 2010; Engel et al., 2001; Varela et al., 2001; Fries, 2005; Engel and Fries, 2010; Siegel et al., 2012), and providing different channels for long-range communication (Bastos et al., 2015; Michalareas et al., 2016). Phase coupling, in particular, has been suggested to serve the routing of information through cortical networks and to promote selective communication between distant brain areas (Engel et al., 2001; Fries, 2005; Womelsdorf et al., 2007). However, how phase coupling supports the brain communication across scales, and how it relates to behavior, is not well understood.

A natural scenario to test the role and mechanisms of phase coupling on brain dynamics at multiple-scales is the integration of multisensory stimuli. In the human brain, studies of multi-scale network dynamics have remained challenging although substantial advances have been made on non-invasive methods such as EEG or MEG. In particular, only a few studies have addressed the relation between phase coupling and multisensory interaction (Keil et al., 2014; Giordano et al., 2017). In animal studies, the potential role of functional connectivity involved in multisensory interactions has so far been investigated only by multielectrode recordings from the same cortical areas (Lakatos et al., 2007; Kayser et al., 2008) or by simultaneous recordings from at most two different regions (Ghazanfar et al., 2008). Neural interactions at short-scales are well established at the level of microcircuits (Coulter et al., 2011; Bastos et al., 2012; Feldmeyer et al., 2013). Invasive studies on

bioRxiv preprint doi: https://doi.org/10.1101/579938; this version posted June 29, 2020. The copyright holder for this preprint (which was not certified by peer review) is the author/funder. All rights reserved. No reuse allowed without permission.

functional connectivity between distant population in behaving animals typically have recorded simultaneously only from relatively small numbers of sites (Womelsdorf and Fries, 2007; Gregoriou et al., 2009; Miller and Buschman, 2013; Liebe et al., 2012; Salazar et al., 2012).

Electrocorticographic (ECoG) arrays offer an option to study simultaneously the relation between multiple-scales of network dynamics and behavior (Ruben et al., 2009; Bosman et al., 2012; Bastos et al., 2015; Stitt et al., 2017). Because of their bio-compatibility and recording stability, they have been used for the study of functional connectivity in networks underlying cognitive and sensorimotor functions (Crone et al., 2006; Bosman et al., 2012; Keller et al., 2014; Fukushima et al., 2015; Lewis et al., 2015) in humans (Canolty and Knight, 2010; Fox et al., 2018), monkeys (Bosman et al., 2012; Bastos et al., 2015) and rodents (Toda et al., 2018).

Here, we have employed an ECoG approach to study large-scale functional connectivity, as reflected in phase coupling of neural oscillations, underlying spatial multisensory processing. We have investigated dynamics during multisensory processing in a large-scale cortical network involving visual, auditory, somatosensory and parietal areas using 64-channel ECoG recordings in behaving ferrets. Animals were trained in a 2-alternative-forced-choice paradigm to detect brief auditory and visual stimuli presented either left or right from the midline. We hypothesized that functional coupling, indicative of dynamic variations in the network state, should be predictive of the animal's performance. While power in hit and miss trials revealed significant differences only around stimulus and response onset, phase coupling already differed between hits and misses at the baseline, suggesting that fluctuations in functional connectivity are an even more important factor that determines task performance. We decomposed the connectivity patterns by principal component analysis to detect the most relevant subnetworks. This showed, in particular, that phase coupling of visual and auditory regions with parietal cortex was predictive of task performance. Our results suggest that fluctuations in the networks state, particular with respect to long-range connectivity, are critical for task performance during multisensory processing.

bioRxiv preprint doi: https://doi.org/10.1101/579938; this version posted June 29, 2020. The copyright holder for this preprint (which was not certified by peer review) is the author/funder. All rights reserved. No reuse allowed without permission.

Materials and Methods

Animals

Data were recorded in four adult female ferrets (*Mustela putorius furo*) trained on a two-alternative forced-choice task involving lateralized detection of visual and auditory stimuli that we have established previously (Hollensteiner et al., 2015). All experiments were approved by the independent Hamburg state authority for animal welfare (BUG-Hamburg) and were performed in accordance with the guidelines of the German Animal Protection Law.

Sensory stimulation

All experiments were carried out in a dark sound-attenuated chamber (Acoustair, Moerkapelle, Netherlands). Visual and auditory stimuli were generated with the Psychophysics Toolbox (Brainard, 1997). Visual stimuli were presented on an LCD monitor (Samsung SyncMaster 2233, frame rate 100 Hz) placed 20 cm in front of the animal. Auditory stimuli were generated digitally with a sample rate of 96 kHz and delivered through two Beyerdynamic T1 speakers. Auditory stimuli consisted of white noise bursts of 100 ms duration and were presented with intensities between 2 to 62 dB SPL. Visual stimuli consisted of circular gratings (22.5 °, 0.2 cycles / °, 5 Hz) with Michelson contrast (Cm) between 0 and 0.38. A static random noise pattern located in the center of the screen was presented to indicate trial onset by a decrease in contrast (not overall luminance). Multisensory stimuli consisted of both stimulation types presented simultaneously.

Training

Initially, ferrets were handled and accustomed to the experimental setup (Fig. 1A). Subsequently, they were trained in the spatial detection task, during which the unimodal as well as crossmodal psychophysical thresholds were estimated. In the task, we used a crossmodal approach that bears on established unimodal training paradigms (e.g. Nodal et al., 2008). Animals were restricted from access to water for a period of 8 hours before the measurements, and conditioned by using water rewards during the task. In the first phase of the study, the animals were trained to detect unimodal auditory and visual stimuli presented in a randomized fashion. Auditory and visual unimodal detection

bioRxiv preprint doi: https://doi.org/10.1101/579938; this version posted June 29, 2020. The copyright holder for this preprint (which was not certified by peer review) is the author/funder. All rights reserved. No reuse allowed without permission.

thresholds were determined using 20 different stimulus amplitudes (auditory: 2-62 dB SPL; visual: 0-0.38 Cm) in a 1 down / 3 up staircase procedure (Kaernbach, 1991). Next, unimodal and bimodal thresholds were assessed in a combined approach, using the previously determined unimodal thresholds to adjust the test parameters (for details of the procedure see Hollensteiner et al., 2015). Subsequently, the ferrets were accustomed to electrophysiological recordings during the detection task with a reduced set of stimulus amplitudes (eight per modality), adjusted to the individual psychometric functions to acquire a higher number of trials in the performance range of interest around 75 % accuracy.

Detection task

The trial schedule of the detection task is shown in Figure 1B. To initialize a trial, the ferret had to maintain a central head position to break the central light-barrier for 500 ms. This caused the static random noise pattern in the center of the screen to decrease in contrast informing the animal that the window for stimulus presentation (from 0 to 1000 ms after trial onset) had started. During this interval, the animal had to further maintain its central head position. A stimulus was presented for 100 ms on either the left or the right side. Stimulus presentation could be unimodal visual ('V'), unimodal auditory ('A') or a temporally congruent bimodal audio-visual stimulus combination. This combination either consisted of a variable auditory stimulus accompanied by a visual stimulus of constant contrast ('Av') or, conversely, a visual stimulus of varying contrast supported by an auditory stimulus of constant amplitude ('Va'). The intensity value of the accompanying second stimulus with constant amplitude was set at a level of 75% accuracy. After stimulus offset, the animal had to respond within 700 ms by moving its head to the stimulated side; otherwise, the trial was considered as a miss (no response). If the response was correct the animal received a water reward (~80 µl) from a spout at the stimulus position and could immediately start the next trial. If the response occurred prematurely (before stimulus onset or within 100 ms after stimulus onset), was incorrect (wrong side) or omitted, the trial was immediately terminated, followed by a 2000 ms interval during which no new trial start could be initialized.

bioRxiv preprint doi: https://doi.org/10.1101/579938; this version posted June 29, 2020. The copyright holder for this preprint (which was not certified by peer review) is the author/funder. All rights reserved. No reuse allowed without permission.

145

146 **Implantation and alignment of ECoG array**

147 Micromachining technology (Rubehn et al., 2009) was used to design and implement an ECoG array
148 that matched the anatomy of the ferret brain (Fig. 2). The thin-film (10 µm) polymide-foil ECoG
149 contained 64 platinum electrodes with a diameter of 250 µm each, arranged in a hexagonal formation
150 at an inter-electrode distance of 1.5 mm.

151 The surgical procedure for the implantation of the ECoG array started with the induction of
152 general anesthesia by using a ketamine-medetomidine mixture (15 mg/kg and 0.08 mg/kg,
153 respectively). During surgery, anesthesia is maintained by applying additional ketamine (20 mg/kg),
154 throughout the implantation procedure the animal was freely breathing. To monitor the state of
155 anesthesia, physiological parameters such as the electrocardiogram (ECG) and rectal temperature were
156 monitored throughout the surgery. All surgical procedures were performed under sterile conditions.
157 After the operating field was prepared, a craniotomy was performed using a saline-cooled ultrasonic
158 microsaw (Mectron) in order to expose the posterior half of the left cerebral hemisphere. The dura was
159 carefully removed and the ECoG array was gently placed on the surface of the cortex such that it
160 covered occipital, temporal and parietal areas (Fig. 2D). The dura was then folded back over the ECoG
161 array and an absorbable artificial dura was placed above the ECoG, covering the trepanation to full
162 extent. The excised piece of bone was fixed back in place with titanium plates and screws and
163 subsequently the gaps were filled with fast set absorbable bone putty. Finally, the ECoG's connector
164 was placed on top of the skull and fixed in place with titanium screws and dental acrylic. After the
165 surgery, the animals received analgesic (carprofen, 4 mg/kg) and antibiotic (enrofloxacin, 5 mg/kg)
166 medication for at least 7 days. To align electrode positions across animals, the ECoG array placement
167 and the cortical parcellation introduced by Bizley et al. (2007) was utilized (Fig. 2B). For each animal,
168 the exact ECoG array position over the posterior cortex was photographically documented during
169 surgery. The locations of all 64 ECoG electrodes were then projected onto a scaled illustration of a
170 ferret model brain. Each electrode was then mapped to the underlying cortical area.

171

172

bioRxiv preprint doi: https://doi.org/10.1101/579938; this version posted June 29, 2020. The copyright holder for this preprint (which was not certified by peer review) is the author/funder. All rights reserved. No reuse allowed without permission.

Electrophysiological recordings

Local field potentials (LFPs) were digitized at 1.4 kHz and sampled simultaneously with a 64-channel AlphaLab SnR recording system (Alpha Omega Engineering, Israel). The high pass filter was set at 0.1 Hz and the low pass filter at 357 Hz.

Data analysis and preprocessing

To reveal dynamic neurophysiological processes along the trial time line, we analyzed spectral power and functional connectivity in the LFPs recorded during the task. To ensure comparability across animals and modalities, only trials with an accuracy of 75±10% were considered in all electrophysiological analyses. Furthermore, this selection of trials ensured better comparability between all four modalities because the value that was fixed during the bimodal stimulation was set at a level of 75% accuracy for all stimulation amplitudes. To assess a sufficient amount of trials with stimulus presentation contralateral to the implanted hemisphere per modality in the 75% accuracy range, trials collected on different days were pooled; see Hollensteiner et al. (2015) for non-stationarity effects across sessions.

All offline data analysis was performed using custom scripts in Matlab (The Mathworks Inc, MA). The hardware-filtered LFP signals were band-pass filtered with a phase-preserving fourth-order Butterworth filter between 2 and 200 Hz. Next, band-stop Butterworth filters at 49-51, 99-101 and 149-151 Hz were applied to notch the line noise. Subsequently, the continuous LFP signals were cut into epochs aligned to trial, stimulus and response onset, respectively. In each of these analysis time windows data was cut from 500 ms pre- to 500 ms post-onset, with 500 ms real data padding on each side to prevent edge artifacts in frequency space. Afterwards, we applied independent component analysis (Hyvärinen and Oja, 2000) to the concatenated analysis window data in order to detect ECG, muscle and eye blink artifacts. Next, we re-referenced the LFP time series of each ECoG contact with the LFP time series of its right neighbor. This processing step created 55 virtual electrodes from the 64 recorded contacts. The virtual electrode position was derived from the difference of both real electrode positions. Subsequently, the oscillatory signal components of unimodal and bimodal trials where analyzed using spectral decomposition.

bioRxiv preprint doi: https://doi.org/10.1101/579938; this version posted June 29, 2020. The copyright holder for this preprint (which was not certified by peer review) is the author/funder. All rights reserved. No reuse allowed without permission.

Spectral power analysis

Channel-wise spectral power was computed by taking the square of the absolute value of the Fourier transform. Spectra were computed for all three analysis time windows using a Hanning window approach (2-200 Hz, 2 Hz steps, 500 ms window; for the LFP spectrogram the window was shifted from – 500 ms to 500 ms around the window of interest) in 1 ms steps.

Functional connectivity

To estimate phase synchronization between ECoG signals, we calculated the phase locking value (PLV; Lachaux et al., 1999) across all frequencies (2-200 Hz). In general, the instantaneous phase was extracted from the analytic signals that were produced by the Fourier transform of the convolution of the ECoG time series with the Hanning window. The PLV between channels A and B at carrier frequency is defined as follows:

$$PLV_{AB}(f) = \frac{1}{N}\left|\sum_{n=1}^{N} e^{i(\theta_n^A(f)-\theta_n^B(f))}\right| \quad (1)$$

For an event related paradigm the circular average of phases is in general non-vanishing, and a non-vanishing result using the classical definition of PLV does not imply statistical dependence between phases in two electrodes. Therefore, we corrected for evoked effects and defined the PLV here as

$$PLV_{AB}(f) = \left|< e^{i(\theta^A(f)-\theta^B(f))} > - < e^{i(\theta^A(f))} >< e^{-i(\theta^B(f))} >\right| \quad (2)$$

Where <> denotes average over trials. For an infinite number of trials, the PLV defined here vanishes exactly if the phase is electrode A and B are statistically independent. To contrast PLV between modalities, we first computed the global mean PLV for the same time windows selected in the spectral power analysis. Subsequently, the PLV between anatomical regions, as defined in Figure 2B, was calculated by averaging across all virtual electrodes overlaying the same area. To normalize and compare PLV values from hit and miss trials we computed the sensitivity index (d'), which is defined by:

bioRxiv preprint doi: https://doi.org/10.1101/579938; this version posted June 29, 2020. The copyright holder for this preprint (which was not certified by peer review) is the author/funder. All rights reserved. No reuse allowed without permission.

$$d' = \frac{\mu_{hit} - \mu_{miss}}{\sqrt{\frac{1}{2}(\sigma_{hit}^2 + \sigma_{miss}^2)}} \quad (3)$$

where μ denotes the mean and σ the standard deviation for hit and miss trials, respectively.

Principal component analysis of functional connectivity

We used a similar approach to Leonardi et al. (2013) to find hidden networks during the baseline period that may be associated to performance by applying principal component analysis (PCA) on trial based connectivity matrices. To facilitate the contrast in the analysis we separated matrices in groups of hits and misses. Before applying PCA, the global mean connectivity matrix was subtracted from matrices of all trials within each group. To avoid redundancy we took only the lower triangular part of each *n*x*n* connectivity matrix (excluding elements of the diagonal) and then vectorized it to obtain a vector of *n(n-1)/2* elements. The vectors of all animals were concatenated along the trial dimension into an array of *(n-1)/2* x*T* elements, with *T* being the total number of trials. PCA was then performed on the resultant matrix. Eigenvectors or principal components (PCs) can be understood as features or subnetworks that characterize the variation across the collection of correlation matrices and represent network patterns. Because these capture connectivity patterns they are also called eigenconnectivities (Leonardi et al., 2013). Finally, to reduce dimensionality and obtain the main eigenconnectivities, matrices were thresholded by the lowest and strongest 10% with respect to their mean.

Directionality analysis

To estimate the direction of causal influences we calculated the phase slope index PSI (Ψ; Nolte et al., 2008). It is highly robust against false estimates caused by confounding factors of very general nature. PSI is defined as follows,

$$\tilde{\Psi}_{ij} = I\left(\sum_{f \in F} C_{ij}^{*}(f) C_{ij}(f + \delta f)\right) \quad (4)$$

bioRxiv preprint doi: https://doi.org/10.1101/579938; this version posted June 29, 2020. The copyright holder for this preprint (which was not certified by peer review) is the author/funder. All rights reserved. No reuse allowed without permission.

where $C_{ij}(f) = S_{ij}(f) / \sqrt{S_{ii} S_{jj}}$ is the complex coherency, S is the cross-spectral matrix, σf is the frequency resolution, and $I(\cdot)$ denotes taking the imaginary part. F is the set of frequencies over which the slope is summed. Finally to normalize $\tilde{\Psi}$ we divided it by its standard deviation

$$\Psi = \tilde{\Psi} / std(\tilde{\Psi}) \quad (5)$$

estimated by the jackknife method. The acquired PSI matrices where thresholded equivalently to the eigenconnectivity matrices and their sign was extracted.

bioRxiv preprint doi: https://doi.org/10.1101/579938; this version posted June 29, 2020. The copyright holder for this preprint (which was not certified by peer review) is the author/funder. All rights reserved. No reuse allowed without permission.

Results

To investigate neural responses and task-related fluctuations of functional connectivity, we recorded local field potentials (LFPs) via 64-channel ECoG arrays chronically implanted in four female ferrets (Hollensteiner et al., 2015).

Multisensory effects on behavior

Before the electrophysiological recordings were conducted, a psychometric evaluation was performed on each animal to determine the parameters (see Methods). Figures 3A and B show examples of psychometric functions fitted to the behavioral data for the A and Av, and for the V and Va conditions, respectively. For further analysis, data were taken only from trials with stimulus intensities at threshold to allow comparisons across conditions and animals (Fig. 3A, B).

Reaction times have been broadly used to quantify differences between unimodal and multisensory stimulation. A *t*-test was run to investigate the differences between Av and A, as well as between Va and V conditions, respectively. Responses to bimodal stimulation were, on average, faster than those to unimodal stimulation ($p < 0.05$). To evaluate whether this effect was driven by the auditory or the visual condition, we computed a repeated one-way analysis of variance (rm-ANOVA), with sensory modality as a main factor. This revealed a main effect of condition (F (3, 12) = 5.3, $p < 0.05$), but post hoc *t*-tests (Bonferroni corrected) only revealed significant differences between the trials of 'A' and all other conditions. The population averages of RTs for Av, Va and V were not significantly different (Fig. 3C). Nevertheless, the population mean RT of V (0.21 sec) was slightly higher than both, Va (0.19 sec) and Av (0.19 sec). The significant difference between the RTs in the A and the Av condition suggest a multisensory interaction effect leading to reduction in RT for the bimodal stimulation. However, our data do not suggest a substantial improvement of visual detection by a concurrent auditory stimulus.

LFP power reflects stimulus processing and response preparation

A major aim of our analysis of the electrophysiological data was to test the relation of power and functional connectivity to task performance by contrasting hit and miss trials. In the hit trial group, we

bioRxiv preprint doi: https://doi.org/10.1101/579938; this version posted June 29, 2020. The copyright holder for this preprint (which was not certified by peer review) is the author/funder. All rights reserved. No reuse allowed without permission.

included all trials with stimulus intensities around 75% threshold and stimulation contralateral to the implanted ECoG (265 ± 14 hit trials per animal). To match the number of hit trials we used all miss trials (236 ± 45 miss trials per animal) throughout all sessions (15 ± 2 sessions per animal). Miss trials were defined as trials with sensory stimulation but without behavioral response, i.e., the ferret maintained the centered head position throughout the response window. The number of false responses, i.e., orientation of the ferret to the side contralateral to the sensory stimulation, were too few and highly variable across animals (104 ± 58 false responses per animal) and, thus, were not considered for analysis of the electrophysiological data.

We hypothesized that spectral characteristics of LFPs immediately before task execution predict the animal's performance. To assess how LFP spectral characteristics evolve during hit, miss and bi- and unimodal stimulation, we computed the power across time windows aligned to baseline, stimulus presentation and response onset for each animal individually (Fig. 4). Results of all animals were pooled after correction for different trial numbers. Power differences between hit and miss trials were analyzed in the theta (4-8 Hz), alpha (8-16 Hz), beta (18-24 Hz), gamma (30-80 Hz) and high-gamma (80 - 160 Hz) frequency band across the analysis time windows (Tab. 1). In addition, one-way ANOVAs were calculated on power values within each frequency band with condition as the main factor to examine differences related to stimulus type (Suppl. Fig. 1; Suppl. Tab. 1).

Figure 4 shows the grand average spectra and time-frequency representation of power changes during each analysis time window (baseline, stimulus and response onset) for hit and miss trials. During the baseline only the high-gamma frequency-band (80 - 160 Hz) showed significant differences with higher power for miss trials ($p < 0.05$; FDR corrected). Comparison of the average spectra in the stimulus onset analysis window showed significant reductions for hit and miss trials in the gamma frequency-range (30 - 160 Hz) compared to baseline (Tab. 1). However, hit trials showed significantly higher power compared to miss trials after stimulus onset in both gamma ($p < 0.001$) and high-gamma ($p < 0.001$) frequency bands (Fig. 4A). Around response onset, hit trials consistently showed significantly higher power compared to miss trials in the theta- ($p < 0.01$), alpha- ($p < 0.01$), gamma- ($p < 0.001$) and high-gamma band ($p < 0.001$). Statistical comparison across analysis time windows within hit- and miss-trials revealed significant de- and increase in the gamma frequency

bioRxiv preprint doi: https://doi.org/10.1101/579938; this version posted June 29, 2020. The copyright holder for this preprint (which was not certified by peer review) is the author/funder. All rights reserved. No reuse allowed without permission.

range compared to baseline and stimulus onset, respectively (Tab. 1; all *p*-values, within and across windows of interest, FDR corrected).

Supplementary Figure 2 shows the topographies of the respective spectral differences between hit and miss trials. In the baseline window, power topographies showed high spatial uniformity across all frequency bands. Around stimulus onset, notable differences occurred mainly in the beta band where, in hit trials, higher beta power occurred in parietal areas. The highest regional differences occurred in the response window. Occipital regions exhibited higher power across all frequency bands during response onset in miss trials compared to hit trials. In contrast, auditory and parietal areas showed increased power in lower frequency bands (theta and alpha) for hit trials. An increase of gamma band power occurred in the response window for hit trials in regions around the lateral sulcus (Suppl. Fig. 2).

To investigate stimulus-type dependent effects within hit-trials a one-way ANOVA between the four conditions (Av, Va, A and V; Suppl. Fig. 1; Suppl. Tab. 1) was calculated. It showed no main effect in the factor condition across frequency bands during baseline, stimulus or response onset. This suggests that power changes related to stimulus processing and response preparation did not depend on the modality of the presented stimulus or on crossmodal interactions.

Functional connectivity predicts performance

To determine whether functional connectivity predicts the animals' performance we computed the PLV between all pairs of ECoG channels for the different frequency bands. PLV analysis was performed for the same time windows, aligned to baseline, stimulus and response onset, respectively, as the power analysis reported above. Figure 5 displays the population average PLV spectra for all hit and miss trials as well as the difference between hits and misses and the relative spectral changes in the stimulus and response onset window relative to baseline. Paired *t*-tests were applied between hit and miss trials within and across all time windows for each frequency band. Within each analysis window, significantly higher PLV was observed for hits compared to miss trials in all frequency bands, with exception of the theta band during response onset ($p < 0.05$, FDR corrected; Fig. 5A).

bioRxiv preprint doi: https://doi.org/10.1101/579938; this version posted June 29, 2020. The copyright holder for this preprint (which was not certified by peer review) is the author/funder. All rights reserved. No reuse allowed without permission.

When compared to the baseline time window, PLV was significantly reduced in the stimulus and response onset windows in nearly all frequency bands. Exceptions were in the theta frequency band for miss trials around stimulus as well as response onset. From stimulus to response onset, there was an increase in alpha PLV and a decrease of gamma PLV for hit trials, as well as a significant decrease in high-gamma PLV for both trial groups (Fig. 5A and Tab. 2).

A one-way ANOVA within analysis time windows and frequency bands with stimulus condition as the main factor revealed significant differences in PLV between stimulation conditions (Av, Va, A and V; Suppl. Fig. 3). During the baseline period there was no significant effects in the main factor condition in the theta frequency band (F (3, 44) = 2.46, $p > 0.05$). However, starting with the alpha (F (3, 76) = 4.98, $p = 0.003$), beta (F (3, 60) = 3.71, $p = 0.016$), gamma (F (3, 412) = 31.89, $p < 0.001$) and high-gamma (F (3, 652) = 56.99, $p < 0.001$) frequency bands, there was a main effect of conditions. This effect persisted also for the windows around stimulus onset (theta: F (3, 44) = 1.23, $p > 0.05$; alpha: F (3, 76) = 3.74, $p = 0.015$; beta: F (3, 60) = 3.5, $p = 0.021$; gamma: F (3, 412) = 26.12, $p < 0.001$; high-gamma: F (3, 652) = 55.67, $p < 0.001$) and response onset (theta: F (3, 44) = 2.31, $p > 0.05$; alpha: F (3, 76) = 3.63, $p = 0.017$; beta: F (3, 60) = 3.67, $p = 0.017$; gamma: F (3, 412) = 25.12, $p < 0.001$; high-gamma: F (3, 652) = 51.24, $p < 0.001$). Furthermore, post-hoc t-test confirmed a constant pattern of significant differences between conditions (Suppl. Tab. 2-4). In particular, for hit trials connectivity was higher in the A and Av conditions than in the V condition, and there was a trend for connectivity in bimodal Va trials to be higher than in unimodal V trials (Suppl. Fig. 3).

In summary, contrasting with the results on power, our analysis of functional connectivity revealed significant differences between hit and miss trials. These differences occurred over a broad range of frequencies across all analysis time windows. While the observed power changes may predominantly reflect differences in local computations within functional systems, the changes observed in PLV indicate large-scale fluctuations in network state involving multiple frequency bands that relate to the animals' performance.

bioRxiv preprint doi: https://doi.org/10.1101/579938; this version posted June 29, 2020. The copyright holder for this preprint (which was not certified by peer review) is the author/funder. All rights reserved. No reuse allowed without permission.

Large-scale coupling shows specific changes during the task

To examine functional connectivity in relation to the topography of cortical areas, we assigned the data of each ECoG contact to a distinct region based on the functional map of cortical areas from Bizley et al. (2007) (see Methods) and constructed functional connectivity matrices accordingly (Fig. 6). Cortical areas were grouped in three functional systems, comprising visual (areas 17, 18, 19, 20, 21), auditory (areas A1, AAF, ADF, PPF and PSF), and parietal areas (SSY, PPc, PPr, S2). Differences between hit and miss trials were expressed using the sensitivity index (d').

In line with the grand average PLV results, the connectivity matrices generally displayed positive d' values and, thus, higher functional connectivity for hit compared to miss trials. (Fig. 6). This effect was most prominent during the baseline window and decreased during the stimulus presentation. For the alpha, gamma and high-gamma band, the PLV difference between hit and miss trials increased again in the response window. Generally, connections between early sensory cortices and parietal cortex displayed the highest differences between hit and miss trials, in particular during the baseline window (Fig. 6; Suppl. Fig. 5).

Eigenconnectivity reveals subnetworks related to performance

To detect subnetworks that mostly contribute to differences in the animal's performance, we examined the baseline period on a single-trial basis by performing PCA for hits and misses along the trial dimension (see Methods). We focused on a subset of areas (18, 19, 21, PPc, PPr, A1 and AAF) from the recorded functional systems for the analysis of task-related subnetworks. The sign of the interactions was extracted from PSI matrices to derive directionality of the coupling in subnetworks.

Figure 7 shows directed eigenconnectivity patterns in the beta and gamma bands for hit and miss trials in the first and second PCs. Only those connections are displayed which had the smallest and the largest differences relative to the mean connectivity in the baseline window (complete matrices and explained variance for PCs 1-6 and all frequency bands are shown in Suppl. Fig. 4). PC1 did not show substantial differences between hits and misses (Fig. 7A; Suppl. Fig. 4). For both hits and misses, the first PC revealed stronger interactions between auditory and visual areas, but weaker interactions between visual and parietal cortices. In contrast, PC2 revealed substantial differences in

bioRxiv preprint doi: https://doi.org/10.1101/579938; this version posted June 29, 2020. The copyright holder for this preprint (which was not certified by peer review) is the author/funder. All rights reserved. No reuse allowed without permission.

functional connectivity between hit and miss trials. These differences were most prominent in the theta, alpha and beta band, but occurred also in the gamma band (Fig. 7B; Suppl. Fig. 4) . In the beta band, coupling within the visual system was stronger for hit compared to miss trials, whereas coupling of auditory area AAF with parietal and visual areas was stronger for hits than for misses (Fig. 7B). Interestingly, an increase in connectivity between AAF and visual areas was a common pattern in miss trials for both PC1 and PC2 in the beta and gamma band (Fig. 7). The third to sixth PCs revealed more complex interaction patterns, with increases as well as decreases for functional connections in both hit and miss trials (Suppl. Fig. 4).

It should be noted that the eigenconnectivity patterns cannot be directly compared to the global connectivity differences between hits and misses described in the preceding sections, because they reflect changes in subnetworks, relative to the average network coupling strength, in the two groups of trials. While higher global connectivity was related to hits and, thus, seems relevant to generate adequate behavior, the eigenconnectivity data suggest that a reduction of coupling in subsets of connections are necessary, possibly for enhancing the distinction between visual and auditory stimuli.

Between- and within-system interactions differ in their relation to behavior

The topography of functional connectivity changes was further analyzed by contrasting between-system and within-system interactions (Fig. 8; Suppl. Fig. 5). For hit trials, interactions between the three functional systems were, on average, stronger than functional connections within the respective system. Regarding the within-system connectivity, the auditory system showed the lowest d'. In the period from baseline to stimulus onset, the strength of d' decreased across all frequency bands. With response onset the spectral profile of d' became more heterogeneous. In the theta-band d' decreased further, whereas it remained unaltered in the beta-band, and increased in the alpha-, gamma- and high-gamma band.

For statistical analysis, we averaged PLV d' values and derived the difference of d' values between long-range (between-system) and short-range (within-system) connectivity and calculated statistics across analysis time windows for each frequency band (Fig. 8; for statistics across systems

bioRxiv preprint doi: https://doi.org/10.1101/579938; this version posted June 29, 2020. The copyright holder for this preprint (which was not certified by peer review) is the author/funder. All rights reserved. No reuse allowed without permission.

and within analysis time windows and frequency see Suppl. Fig. 5 and Suppl. Tab. 5; for condition specific statistics see Suppl. Fig. 6). To reveal dynamic effects within frequency bands of interest a one-way ANOVA with time window as the main factor was computed. There was no main effect in the theta band (F (2, 6) = 4.39, $p > 0.05$). The ANOVA exposed significant effects for the main factor time window (alpha (F (2, 12) = 17.17, $p < 0.001$; beta (F (2, 9) = 14.43, $p = 0.002$; gamma (F (2, 75) = 3.71, $p < 0.001$; high-gamma (F (2, 120) = 17.94, $p < 0.001$). Post hoc t-tests revealed significant differences between baseline and stimulus onset for all frequency bands with the main effect (alpha: $p = 0.011$; beta: $p = 0.002$; gamma: $p < 0.001$; high-gamma: $p < 0.001$), between stimulus and response onset for the gamma frequency range (gamma: $p = 0.009$; high-gamma: $p < 0.001$) and between baseline and response onset in the alpha- ($p < 0.001$) and beta- ($p = 0.006$) frequency bands (Bonferroni corrected).

Overall, comparison of functional connectivity between and within cortical systems across the different analysis time windows revealed that between- compared to within-system connectivity was stronger during the task period compared to the pre-stimulus baseline. In hit trials, phase coupling was higher between systems in the gamma frequency range during stimulus onset compare to baseline and response onset. Furthermore, low frequency (alpha and beta) coupling between systems increased around response onset in hit trials compared to miss trials. These results suggest that fluctuations in the network state, particularly with respect to long-range connectivity, are related to task performance.

bioRxiv preprint doi: https://doi.org/10.1101/579938; this version posted June 29, 2020. The copyright holder for this preprint (which was not certified by peer review) is the author/funder. All rights reserved. No reuse allowed without permission.

Discussion

This study has aimed at investigating the cortical network dynamics underlying performance in a multisensory detection task. The main focus of our analysis was on the relation between functional connectivity and task performance. We have used an ECoG approach to record a large-scale network comprising visual, auditory, somatosensory and parietal areas in behaving animals over extended time periods. We hypothesized that fluctuations in power and coupling, indicative of dynamic variations in the network state, should be predictive of the animals' performance. In line with this hypothesis, our data show that pre-trial baseline connectivity predicts the animals' performance, suggesting that fluctuations in coupling across the network lead to variability in behavior. In contrast, local signal power in the pre-trial baseline does not predict hits and misses. Analysis of the topography of connectivity differences between hits and misses suggested specific patterns. In particular, higher global phase coupling of visual and auditory regions to parietal cortex was predictive of task performance, yet a reduction in connectivity in certain subnetworks may be necessary for distinct functional systems to detect stimuli appropriately. Furthermore, we analyzed the ratio between long- and short-range functional connectivity across the different task phases. We observed that long-range coupling became more predominant during the task period compared to the pre-stimulus baseline and changed its spectral profile over the course of the trials.

Relating large-scale connectivity to task performance

The key goal of this study was to investigate the relation between phase coupling and performance of the animal in the detection task with the aim to provide further evidence for the functional relevance of dynamic coupling across cortical populations. A number of different approaches have been used to capture the relation between large-scale connectivity and task performance. In humans, phase coupling has been increasingly studied using EEG or MEG in recent years (Fell and Axmacher, 2011; Siegel et al., 2012; O'Neill et al., 2017). Coherence of different brain areas has been observed during cognitive tasks involving perceptual selection (Hipp et al 2011), attentional selection (Siegel et al., 2008; Michalareas et al., 2016), working memory (Brookes et al., 2011) or speech processing (Giraud and Poeppel, 2012; Giordano et al., 2017). Animal studies have demonstrated a relation of long-range

bioRxiv preprint doi: https://doi.org/10.1101/579938; this version posted June 29, 2020. The copyright holder for this preprint (which was not certified by peer review) is the author/funder. All rights reserved. No reuse allowed without permission.

phase coupling in various frequency ranges to sensorimotor processing, attentional selection and working memory (Bernasconi et al., 2000; Roelfsema et al., 1997; Gregoriou et al., 2009; Salazar et al., 2012; Liebe et al., 2012; Bosman et al., 2012; Saalmann et al., 2012; Bastos et al., 2015).

Despite the fact that the ECoG array in this study covered only the posterior half of one cortical hemisphere, it enabled us to record from an extended network of cortical areas involving visual, auditory, somatosensory and parietal areas. This allowed us to investigate large-scale network dynamics during trained behavior over a large number of recording sessions. A key feature in the present study was the ability to simultaneously monitor several different functional systems, while also allowing recordings from multiple areas within the same cortical system. This approach enabled a systematic comparison of within-system and between-system spectral properties as a function of the animals' behavior.

Our results show that phase coupling, in contrast to local power, is already different between hit and miss trials in the pre-trial baseline, suggesting that fluctuations in network state may be an imported factor that determines task performance. The data indicate that stronger phase coupling in the network may lead to higher efficiency of stimulus processing and response preparation. This is in line with earlier studies that have demonstrated that increased synchrony enhances communication across brain areas (e.g., in the context of attention: Fries, 2005; Bosman et al., 2012) supporting the role of functional connectivity in linking task-relevant modalities to areas involved in selection of responses (Siegel et al., 2012; Miller and Buschman, 2013). Indeed, we find that stronger phase coupling of early sensory to parietal areas was predictive of task performance.

Contrary to earlier studies, we did not observe the typical vigilance- or attention-related signatures in pre-stimulus functional connectivity characterized by increases in high frequency and decreases in low frequency bands (Hanslmayr et al., 2007; Siegel et al., 2008; Bosman et al., 2012). Although the average connectivity differences between hits and misses had a rather broad spectral profile, analysis of the ratio between long-range (between cortical systems) and local (within cortical systems) interactions revealed spectral shifts in this ratio between the task period and the pre-stimulus baseline. In hit trials, between-system phase coupling in the gamma frequency range was higher during stimulus onset compared to baseline and response onset. In contrast, in low frequency (alpha

bioRxiv preprint doi: https://doi.org/10.1101/579938; this version posted June 29, 2020. The copyright holder for this preprint (which was not certified by peer review) is the author/funder. All rights reserved. No reuse allowed without permission.

and beta) ranges between-system coupling increased around response onset in hit trials compared to miss trials. Although we did not employ directed connectivity measures such as Granger causality to distinguish between bottom-up and top-down information flows (Bastos et al., 2015), these data suggest the possibility that, during stimulus processing, interactions within higher frequencies predominate in successful trials, which might reflect stronger bottom-up signaling. This could relate to attentional gating, allowing information to pass through the network to higher areas. In contrast, the predominance of low-frequency interactions in the epoch around response onset might indicate stronger top-down information flow (Bastos et al., 2015). Alternatively, in that phase of the trial, parts of the network could already return to a default state dominated by low frequency oscillations. Averaged across areas, spectral differences between connections with dominant bottom-up and top-down information flows, might even out and, thus, yield the broad spectral profile of connectivity changes observed in the present analysis.

Functional connectivity and multisensory processing

As discussed above, dynamic functional coupling likely constitutes a mechanism for integration of distributed neural signals and sensory systems (Singer and Gray, 1995; Engel et al., 2001; Fries, 2005; Arnal et al., 2015; Ploner et al., 2017). It has been suggested that similar mechanisms might operate for the integration of information across different sensory systems. Thus, multisensory interactions might involve dynamic coupling of oscillatory signals arising in different cortical systems (Senkowski et al., 2008; Talsma et al., 2010). In the human brain, the vast majority of studies on neural oscillations and crossmodal processing have focused on local power changes, and only few investigations have addressed the relation between multisensory processing and functional coupling (Keil et al., 2014; Giordano et al., 2017). Using a data-driven approach for analysis of functional coupling in the human EEG, we could recently demonstrate that coherence in networks involving parietal and sensorimotor areas predicts performance in a visuotactile matching task (Wang et al., 2018). Simultaneous recordings from auditory cortex and superior temporal sulcus in the monkey have revealed increased coherence during congruent auditory and visual stimulation (Maier et al., 2008; Ghazanfar et al., 2008). While these in-vivo studies investigated multisensory interactions only by recordings from the

bioRxiv preprint doi: https://doi.org/10.1101/579938; this version posted June 29, 2020. The copyright holder for this preprint (which was not certified by peer review) is the author/funder. All rights reserved. No reuse allowed without permission.

same cortical areas or by simultaneous recordings from at most two different regions, our study has addressed multisensory networks at a larger scale involving visual, auditory and parietal cortical regions. While our data clearly demonstrate a relation of functional connectivity to task performance, we did not obtain evidence for stimulus-specific changes of coupling between visual and auditory areas, resembling recent results in anesthetized ferrets (Galindo-Leon et al., 2019), where modification of coupling structure occurred only on longer time scales and not in a stimulus-related manner.

The absence of profound connectivity effects related to multisensory interaction may relate to the nature of the task used in our study, which did not require integration of features across modalities, but only the rapid detection of highly transient stimuli. Nonetheless, our results on connectivity data support the notion that significant functional coupling can occur already between early sensory areas, suggesting that multisensory integration can already occur at early processing stages and does not solely rely on binding of information at higher processing levels (Bizley et al., 2007; Lakatos et al., 2007; Senkowski et al., 2008). This is in line with anatomical data suggesting that direct projections from primary auditory to visual cortices can enable functional coupling supporting early multisensory interactions (Bizley et al., 2015).

Network state and behavioral variability

A key result of our study is that phase coupling differed between hit and miss trials already in ongoing activity in the baseline period. The local power in this period did not differ between hits and misses. Our data suggest that fluctuations in the network state occur which lead to variability in the animals' behavior, and that these state changes are primarily reflected in shifts of long-range connectivity, rather than changes in the dynamics of local populations. Early studies assumed that ongoing neural activity corresponds to noise resulting from random signal fluctuations without any functional relevance (Zohary et al., 1994; Shadlen et al., 1996). However, this view has been challenged by evidence showing that ongoing activity carries information that can shape sensory and cognitive processing (Arieli et al., 1996; Fries et al., 2001; Engel et al., 2001; Busch et al., 2009; Keil et al., 2014; Galindo-Leon et al., 2019). Such fluctuations of ongoing activity do not occur only locally, but

bioRxiv preprint doi: https://doi.org/10.1101/579938; this version posted June 29, 2020. The copyright holder for this preprint (which was not certified by peer review) is the author/funder. All rights reserved. No reuse allowed without permission.

551 are strongly synchronized across spatially distributed neuronal populations (Steriade et al., 1996; Stitt
552 et al., 2017; Fischer et al., 2018; Galindo-Leon et al., 2019).

553 Phase coupling of oscillations in pre-stimulus epochs has been shown both in animal and
554 human studies to predict perception and performance in cognitive tasks. For instance, studies in
555 monkey visual cortex indicate that fluctuations in gamma-band phase coupling modulates the speed at
556 which animals can detect a behaviorally-relevant stimulus change (Womelsdorf et al., 2006). EEG
557 studies in humans provide convergent evidence that pre-stimulus fluctuations in phase coupling can
558 modulate target detection (Hanslmayr et al., 2007). Furthermore, intrinsic fluctuations of phase
559 coupling are associated with fluctuations in perceptual states in ambiguous stimulus settings.
560 Fluctuations in beta-band or gamma-band phase coupling have been shown to predict the perceptual
561 state in ambiguous sensory paradigms (Rose and Büchel, 2005; Hipp et al., 2011) and decision making
562 in near-threshold stimulation regimes (Donner et al., 2009). Our current results corroborate and extend
563 this evidence by showing that, at perceptual threshold, detection of the lateralized stimuli by the
564 animals is biased by phase coupling in the pre-stimulus interval.

565 A crucial element in our approach is the ability to simultaneously monitor numerous cortical
566 areas, enabling us to quantify within-system and between-system interactions and to characterize these
567 in a spectrally resolved manner. Our analysis showed that, in particular, long-range connectivity
568 between different functional systems was related to successful stimulus detection. This is in line with
569 the hypothesis that long-range phase coupling may serve efficient transmission of task-relevant
570 information in sensorimotor networks (Engel et al., 2001; Fries, 2005; Womelsdorf et al., 2007).
571 However, the variations in connectivity patterns associated to changes in behavioral performances, do
572 not occur arbitrarily along the whole cortex, but in specific subnetworks, or also termed principal
573 components of functional connectivity. Whether these subnetworks are associated to a decision
574 making network, or rather sensory processing is not clear. However, since most of the nodes include
575 primary sensory areas, we speculate that the reason for miss trials is a sub-optimal function of stimulus
576 coding.

577 Our results also support the view that the characterization of changes in brain-state strongly
578 benefits from inclusion of connectivity analyses. The observation that changes in network state are

bioRxiv preprint doi: https://doi.org/10.1101/579938; this version posted June 29, 2020. The copyright holder for this preprint (which was not certified by peer review) is the author/funder. All rights reserved. No reuse allowed without permission.

reflected, in particular in fluctuations of large-scale connectivity, is in line with results of other recent studies. Supportive evidence has been obtained in studies on the human brain (He et al., 2008; Supp et al., 2011). Using the same ECoG recording approach for the study of ongoing activity, we have observed that functional connectivity shows state-dependent reconfiguration which can also involve shifts in the ratio between short- and long-range interactions (Stitt et al., 2017; Fischer et al., 2018). These findings raise the question of possible mechanisms that might modulate large-scale functional connectivity in a state- and task-dependent manner. Possible candidates are changes in the output of ascending neuromodulatory systems (Harris and Thiele, 2011). Phase coupling has long been known to be influenced by neuromodulators (Steriade et al., 1993). For instance, activation of cholinergic brain stem nuclei has been shown to enhance gamma-band phase coupling in cortical networks (Munk et al., 1996). Neuropharmacological evidence suggests, furthermore, that noradrenergic brain stem inputs can modulate large-scale functional connectivity in cortex (van den Brink et al., 2018).

Conclusion

Our study has demonstrated functional coupling across visual, auditory and parietal areas during a lateralized detection task in the ferret. Analysis of power for hit and miss trials revealed significant differences around stimulus and response onset. In contrast, phase coupling already differed between hits and misses at baseline, suggesting an essential role of large-scale functional connectivity in the animal's ability to perform the task. In particular, higher phase coupling of visual and auditory regions to parietal cortex was predictive of task performance. We observed that long-range coupling became more predominant during the task period compared to the pre-stimulus baseline. Taken together, these results suggest that fluctuations in the network state, particular with respect to long-range connectivity, are critical determinants of the animals' behavior. Future studies might address the relation to the underlying structural connectivity and the mechanisms that give rise to the observed variability of phase coupling.

bioRxiv preprint doi: https://doi.org/10.1101/579938; this version posted June 29, 2020. The copyright holder for this preprint (which was not certified by peer review) is the author/funder. All rights reserved. No reuse allowed without permission.

Acknowledgements

We would like to thank Dorrit Bystron for her assistance throughout experiments. This research was supported by funding from the DFG (SFB 936/A2, SPP 1665/EN533/13-1, SPP 2041/EN533/15-1, A.K.E.; SFB936/Z3, G.N.).

Competing Interests

They are no competing interests.

Author Contributions

K.J.H, F.P. and A.K.E. conceived and designed experiments. G.E. wrote animal ethics permission. K.J.H and F.P. surgically implanted arrays. K.J.H. performed experiments. K.J.H., F.P., E.G.L. and G.N. provided analyzing tools. K.J.H. analyzed data. K.J.H., E.G.L. and A.K.E. wrote the paper. All authors edited and approved the manuscript.

bioRxiv preprint doi: https://doi.org/10.1101/579938; this version posted June 29, 2020. The copyright holder for this preprint (which was not certified by peer review) is the author/funder. All rights reserved. No reuse allowed without permission.

References

Alais D, Newell FN, Mamassian P. 2010. Multisensory processing in review: From physiology to behaviour. *Seeing Perceiving* **23**:3–38. doi:10.1163/187847510X488603

Arieli A, Sterkin A, Grinvald A, Aertsen A. 1996. Dynamics of ongoing activity: Explanation of the large variability in evoked cortical responses. *Science* **273**:1868–1871. doi:10.1126/science.273.5283.1868

Arnal LH, Poeppel D, Giraud AL. 2015. Temporal coding in the auditory cortex. *Handb Clin Neurol* **129**:85–98. doi:10.1016/B978-0-444-62630-1.00005-6

Bastos AM, Usrey WM, Adams RA, Mangun GR, Fries P, Friston KJ. 2012. Canonical microcircuits for predictive coding. *Neuron* **76**:695–711. doi:10.1016/j.neuron.2012.10.038

Bastos AM, Vezoli J, Bosman CA, Schoffelen J-M, Oostenveld R, Dowdall JR, De Weerd P, Kennedy H, Fries P. 2015. Visual areas exert feedforward and feedback influences through distinct frequency channels. *Neuron* **85**:390–401. doi:10.1016/j.neuron.2014.12.018

Bernasconi C, von Stein A, Chiang C, König P. 2000. Bi-directional interactions between visual areas in the awake behaving cat. *Neuroreport* **11**:689–692. doi:10.1097/00001756-200003200-00007

Bizley JK, Nodal FR, Bajo VM, Nelken I, King AJ. 2007. Physiological and anatomical evidence for multisensory interactions in auditory cortex. *Cereb Cortex* **17**:2172–2189. doi:10.1093/cercor/bhl128

Bizley, K, Bajo VM, Nodal FR, King AJ. 2015. Cortico-cortical connectivity within ferret auditory cortex. *J Comp Neurol* **523**: 2187–2210. doi:10.1002/cne.23784

Bosman CA, Schoffelen J-M, Brunet N, Oostenveld R, Bastos AM, Womelsdorf T, Rubehn B, Stieglitz T, De Weerd P, Fries P. 2012. Attentional stimulus selection through selective synchronization between monkey visual areas. *Neuron* **75**:875–888. doi:10.1016/j.neuron.2012.06.037

Brainard DH. 1997. The psychophysics toolbox. *Spat Vis* **10**:433–436. doi:10.1163/156856897X00357

bioRxiv preprint doi: https://doi.org/10.1101/579938; this version posted June 29, 2020. The copyright holder for this preprint (which was not certified by peer review) is the author/funder. All rights reserved. No reuse allowed without permission.

644 Brookes MJ, Wood JR, Stevenson CM, Zumer JM, White TP, Liddle PF, Morris PG. 2011. Changes
645 in brain network activity during working memory tasks: A magnetoencephalography study.
646 *NeuroImage* **55**:1804–1815. doi: 10.1016/j.neuroimage.2010.10.074
647 Busch NA, Dubois J, VanRullen R. 2009. The phase of ongoing EEG oscillations predicts visual
648 perception. *J Neurosci* **29**:7869–7876. doi:10.1523/JNEUROSCI.0113-09.2009
649 Buzsaki G. 2006. Rhythms of the brain. Oxford University Press.
650 Canolty RT, Knight RT. 2010. The functional role of cross-frequency coupling. *Trends Cogn Sci*
651 **14**:506–515. doi:10.1016/j.tics.2010.09.001
652 Coulter DA, Yue C, Ang CW, Weissinger F, Goldberg E, Hsu F-C, Carlson GC, Takano H. 2011.
653 Hippocampal microcircuit dynamics probed using optical imaging approaches. *J Physiol*
654 **589**:1893–1903. doi:10.1113/jphysiol.2010.202184
655 Crone NE, Sinai A, Korzeniewska A. 2006. High-frequency gamma oscillations and human brain
656 mapping with electrocorticography. *Prog Brain Res* **159**:275–295. doi:10.1016/S0079-
657 6123(06)59019-3
658 Donner TH, Siegel M, Fries P, Engel AK. 2009. Build-up of choice-predictive activity in human
659 motor cortex during perceptual decision making. *Curr Biol* **19**: 1581–1585.
660 doi:10.1016/j.cub.2009.07.066
661 Engel AK, Fries P. 2010. Beta-band oscillations--signalling the status quo? *Curr Opin Neurobiol*
662 **20**:156–165. doi:10.1016/j.conb.2010.02.015
663 Engel AK, Fries P, Singer W. 2001. Dynamic predictions: Oscillations and synchrony in top–down
664 processing. *Nat Rev Neurosci* **2**:704–716. doi:10.1038/35094565
665 Engel AK, Gerloff C, Hilgetag CC, Nolte G. 2013. Intrinsic coupling modes: Multiscale interactions
666 in ongoing brain activity. *Neuron* **80**:867–886. doi:10.1016/j.neuron.2013.09.038
667 Feldmeyer D, Brecht M, Helmchen F, Petersen CCH, Poulet JFA, Staiger JF, Luhmann HJ, Schwarz
668 C. 2013. Barrel cortex function. *Prog Neurobiol* **103**:3–27.
669 doi:10.1016/j.pneurobio.2012.11.002
670 Fell J, Axmacher N. 2011. The role of phase synchronization in memory processes. *Nat Rev Neurosci*
671 **12**:105–118. doi:10.1038/nrn2979

bioRxiv preprint doi: https://doi.org/10.1101/579938; this version posted June 29, 2020. The copyright holder for this preprint (which was not certified by peer review) is the author/funder. All rights reserved. No reuse allowed without permission.

672 Fischer F, Pieper F, Galindo-Leon E, Engler G, Hilgetag CC, Engel AK. 2018. Intrinsic functional
673 connectivity resembles cortical architecture at various levels of isoflurane anesthesia. *Cereb*
674 *Cortex* **28**:2991–3003. doi:10.1093/cercor/bhy114
675 Fox KCR, Foster BL, Kucyi A, Daitch AL, Parvizi J. 2018. Intracranial electrophysiology of the
676 human default Network." *Trends Cogn Sci* **22**: 307–324. doi:10.1016/j.neuron.2007.08.023
677 Fries P, Neuenschwander S, Engel AK, Goebel R, Singer W. 2001. Rapid feature selective neuronal
678 synchronization through correlated latency shifting. *Nat Neurosci* **4**: 194–200.
679 doi:10.1038/84032
680 Fries P. 2005. A mechanism for cognitive dynamics: Neuronal communication through neuronal
681 coherence. *Trends Cogn Sci* **9**:474–480. doi:10.1016/j.tics.2005.08.011
682 Fukushima M, Chao ZC, Fujii N. 2015. Studying brain functions with mesoscopic measurements:
683 Advances in electrocorticography for non-human primates. *Curr Opin Neurobiol* **32**:124–131.
684 doi:10.1016/j.conb.2015.03.015
685 Galindo-Leon, E., Stitt, I., Pieper, F., Stieglitz, T., Engler, G., Engel, A.K., 2019. Context-specific
686 modulation of intrinsic coupling modes shapes multisensory processing. *Sci Adv* **5**: eaar7633.
687 509943. doi: 10.1126/sciadv.aar7633
688 Ghazanfar AA, Chandrasekaran C, Logothetis NK. 2008. Interactions between the superior temporal
689 sulcus and auditory cortex mediate dynamic face/voice integration in rhesus monkeys. *J*
690 *Neurosci* **28**:4457–4469. doi:10.1523/JNEUROSCI.0541-08.2008
691 Giordano BL, Ince RAA, Gross J, Schyns PG, Panzeri S, Kayser C. 2017. Contributions of local
692 speech encoding and functional connectivity to audio-visual speech perception. *eLife* **6**.
693 doi:10.7554/eLife.24763
694 Giraud A-L, Poeppel D. 2012. Cortical oscillations and speech processing: Emerging computational
695 principles and operations. *Nat Neurosci* **15**:511–517. doi:10.1038/nn.3063
696 Green AM, Angelaki DE. 2010. Multisensory integration: Resolving sensory ambiguities to build
697 novel representations. *Curr Opin in Neurobiol* **20**:353–360. doi:10.1016/j.conb.2010.04.009

bioRxiv preprint doi: https://doi.org/10.1101/579938; this version posted June 29, 2020. The copyright holder for this preprint (which was not certified by peer review) is the author/funder. All rights reserved. No reuse allowed without permission.

698 Gregoriou GG, Gotts SJ, Zhou H, Desimone R. 2009. High-frequency, long-range coupling between
699 prefrontal and visual cortex during attention. *Science* **324**:1207–1210.
700 doi:10.1126/science.1171402
701 Hanslmayr S, Aslan A, Staudigl T, Klimesch W, Herrmann CS, Bäuml K-H. 2007. Prestimulus
702 oscillations predict visual perception performance between and within subjects. *NeuroImage*
703 **37**:1465–1473. doi:10.1016/j.neuroimage.2007.07.011
704 Harris KD, Thiele A. 2011. Cortical state and attention. *Nat Rev Neurosci* **12**:509–523.
705 doi:10.1038/nrn3084
706 He BJ, Snyder AZ, Zempel JM, Smyth MD, Raichle ME. 2008. Electrophysiological correlates of the
707 brain's intrinsic large-scale functional architecture. *Proc Natl Acad Sci USA* **105**: 16039–
708 16044. doi:10.1101/pdb.top078147
709 Hipp JF, Engel AK, Siegel M. 2011. Oscillatory synchronization in large-scale cortical networks
710 predicts perception. *Neuron* **69**:387–396. doi:10.1016/j.neuron.2010.12.027
711 Hollensteiner KJ, Pieper F, Engler G, König P, Engel AK. 2015. Crossmodal integration improves
712 sensory detection thresholds in the ferret. *PLoS One* **10**:e0124952. doi:
713 10.1371/journal.pone.0124952
714 Hyvärinen A, Oja E. 2000. Independent component analysis: Algorithms and applications. *Neural*
715 *Netw* **13**:411–430. doi:10.1016/S0893-6080(00)00026-5
716 Jensen O, Mazaheri A. 2010. Shaping functional architecture by oscillatory alpha activity: Gating by
717 inhibition. *Front Hum Neurosci* **4**. doi:10.3389/fnhum.2010.00186
718 Kaernbach C. 1991. Simple adaptive testing with the weighted up-down method. *Perception &*
719 *Psychophysics* **49**:227–229. doi:10.3758/BF03214307
720 Kayser C, Petkov CI, Logothetis NK. 2008. Visual modulation of neurons in auditory cortex. *Cereb*
721 *Cortex* **18**:1560–1574. doi:10.1093/cercor/bhm187
722 Keil J, Müller N, Hartmann T, Weisz N. 2014. Prestimulus beta power and phase synchrony influence
723 the sound-induced flash illusion. *Cereb Cortex* **24**:1278–1288. doi:10.1093/cercor/bhs409

bioRxiv preprint doi: https://doi.org/10.1101/579938; this version posted June 29, 2020. The copyright holder for this preprint (which was not certified by peer review) is the author/funder. All rights reserved. No reuse allowed without permission.

724 Keller CJ, Honey CJ, Mégevand P, Entz L, Ulbert I, Mehta AD. 2014. Mapping human brain networks
725 with cortico-cortical evoked potentials. *Philos Trans R Soc B Biol Sci* **369**:20130528.
726 doi:10.1098/rstb.2013.0528
727 Lachaux JP, Rodriguez E, Martinerie J, Varela FJ. 1999. Measuring phase synchrony in brain signals.
728 *Hum Brain Mapp* **8**:194–208. doi:10.1002/(SICI)1097-0193(1999)8:4<194::AID-
729 HBM4>3.0.CO;2-C
730 Lakatos P, Chen C-M, O'Connell MN, Mills A, Schroeder CE. 2007. Neuronal oscillations and
731 multisensory interaction in primary auditory cortex. *Neuron* **53**:279–292.
732 doi:10.1016/j.neuron.2006.12.011
733 Leonardi, N., Richiardi, J., Gschwind, M., Simioni, S., Annoni, J.-M., Schluep, M., Vuilleumier, P.,
734 Van De Ville, D., 2013. Principal components of functional connectivity: A new approach to
735 study dynamic brain connectivity during rest. *NeuroImage* **83**:937–950.
736 doi:10.1016/j.neuroimage.2013.07.019
737 Lewis C, Bosman C, Fries P. 2015. Recording of brain activity across spatial scales. *Curr Opin*
738 *Neurobiol* **32**:68–77. doi:10.1016/j.conb.2014.12.007
739 Liebe S, Hoerzer GM, Logothetis NK, Rainer G. 2012. Theta coupling between V4 and prefrontal
740 cortex predicts visual short-term memory performance. *Nature Neuroscience* **15**:456–462.
741 doi:10.1038/nn.3038
742 Maier JX, Chandrasekaran C, Ghazanfar AA. 2008. Integration of bimodal looming signals through
743 neuronal coherence in the temporal lobe. *Curr Biol* **18**:963–968.
744 doi:10.1016/j.cub.2008.05.043
745 Michalareas G, Vezoli J, van Pelt S, Schoffelen J-M, Kennedy H, Fries P. 2016. Alpha-beta and
746 gamma rhythms subserve feedback and feedforward influences among human visual cortical
747 areas. *Neuron* **89**:384–397. doi:10.1016/j.neuron.2015.12.018
748 Miller EK, Buschman TJ. 2013. Cortical circuits for the control of attention. *Curr Opin Neurobiol*
749 **23**:216–222. doi:10.1016/j.conb.2012.11.011

bioRxiv preprint doi: https://doi.org/10.1101/579938; this version posted June 29, 2020. The copyright holder for this preprint (which was not certified by peer review) is the author/funder. All rights reserved. No reuse allowed without permission.

Munk MH, Roelfsema PR, König P, Engel AK, Singer W. 1996. Role of reticular activation in the modulation of intracortical synchronization. *Science* **272**: 271–274. doi:10.1126/science.272.5259.271

Nodal FR, Bajo VM, Parsons CH, Schnupp JW, King AJ. 2008. Sound localization behavior in ferrets: Comparison of acoustic orientation and approach-to-target responses. *Neuroscience* **154**:397–408. doi:10.1016/j.neuroscience.2007.12.022

Nolte G, Ziehe A, Nikulin VV., Schlögl A, Krämer N, Brismar T, Müller KR 2008. "Robustly Estimating the Flow Direction of Information in Complex Physical Systems." *Physical Review Letters* 100, **23**: 234101. doi:10.1103/PhysRevLett.100.234101

O'Neill GC, Tewarie PK, Colclough GL, Gascoyne LE, Hunt BAE, Morris PG, Woolrich MW, Brookes MJ. 2017. Measurement of dynamic task related functional networks using MEG. *NeuroImage* **146**:667–678. doi:10.1016/j.neuroimage.2016.08.061

Ploner M, Sorg C, Gross J. 2017. Brain rhythms of pain. *Trends Cogn Sci* **21**: 100–110. doi:10.1016/j.tics.2016.12.001

Raichle ME. 2010. Two views of brain function. *Trends Cogn Sci* **14**:180–190. doi:10.1016/j.tics.2010.01.008

Roelfsema PR, Engel AK, König P, Singer W. 1997. Visuomotor integration is associated with zero time-lag synchronization among cortical areas. *Nature* **385**:157-161. doi:10.1038/385157a0

Rose M, Büchel C. 2005. Neural coupling binds visual tokens to moving stimuli. *J Neurosci* **25**: 10101–10104. doi:10.1523/JNEUROSCI.2998-05.2005

Rubehn B, Bosman C, Oostenveld R, Fries P, Stieglitz T. 2009. A MEMS-based flexible multichannel ECoG-electrode array. *J Neural Eng* **6**:036003. doi:10.1088/1741-2560/6/3/036003

Saalmann YB, Pinsk MA, Wang L, Li X, Kastner S. 2012. The pulvinar regulates information transmission between cortical areas based on attention demands. *Science* **337**:753–756. doi:10.1126/science.1223082

Salazar RF, Dotson NM, Bressler SL, Gray CM. 2012. Content-specific fronto-parietal synchronization during visual working memory. *Science* **338**:1097–1100. doi:10.1126/science.1224000

bioRxiv preprint doi: https://doi.org/10.1101/579938; this version posted June 29, 2020. The copyright holder for this preprint (which was not certified by peer review) is the author/funder. All rights reserved. No reuse allowed without permission.

778 Senkowski D, Schneider TR, Foxe JJ, Engel AK. 2008. Crossmodal binding through neural
779 coherence: implications for multisensory processing. *Trends Neurosci* **31**:401–409.
780 doi:10.1016/j.tins.2008.05.002
781 Shadlen MN, Britten KH, Newsome WT, Movshon JA. 1996. A computational analysis of the
782 relationship between neuronal and behavioral responses to visual motion. *J Neurosci* **16**:1486–
783 1510. doi:10.1523/JNEUROSCI.16-04-01486.1996
784 Siegel M, Donner TH, Engel AK. 2012. Spectral fingerprints of large-scale neuronal interactions. *Nat*
785 *Rev Neurosci* **13**:121–134. doi:10.1038/nrn3137
786 Siegel M, Donner TH, Oostenveld R, Fries P, Engel AK. 2008. Neuronal synchronization along the
787 dorsal visual pathway reflects the focus of spatial attention. *Neuron* **60**: 709-719.
788 doi:10.1016/j.neuron.2008.09.010
789 Singer W, Gray CM. 1995. Visual feature integration and the temporal correlation hypothesis. *Annu*
790 *Rev Neurosci* **18**:555–586. doi:10.1146/annurev.ne.18.030195.003011
791 Stein BE, Meredith A. 1993. The merging of the senses. Cambridge, Mass.: MIT Press.
792 Steriade M, Contreras D, Amzica F, Timofeev I. 1996. Synchronization of fast (30-40 Hz)
793 spontaneous oscillations in intrathalamic and thalamocortical networks. *J Neurosci* **16**:2788–
794 2808. doi:10.1523/JNEUROSCI.16-08-02788.1996
795 Steriade M, McCormick DA, Sejnowski TJ (1993) Thalamocortical oscillations in the sleeping and
796 aroused brain. *Science* **262**: 679–685. doi:10.1126/science.8235588
797 Stitt I, Hollensteiner KJ, Galindo-Leon E, Pieper F, Fiedler E, Stieglitz T, Engler G, Nolte G, Engel
798 AK. 2017. Dynamic reconfiguration of cortical functional connectivity across brain states. *Sci*
799 *Rep* **7**:8797. doi:10.1038/s41598-017-08050-6
800 Supp GG, Siegel M, Hipp JF, Engel AK. 2011. Cortical hypersynchrony predicts breakdown of
801 sensory processing during loss of consciousness." *Curr Biol* **21**: 1988–1993.
802 doi:10.1016/j.cub.2011.10.017
803 Talsma D, Senkowski D, Soto-Faraco S, Woldorff MG. 2010. The multifaceted interplay between
804 attention and multisensory integration. *Trends Cogn Sci* **14**:400–410.
805 doi:10.1016/j.tics.2010.06.008

bioRxiv preprint doi: https://doi.org/10.1101/579938; this version posted June 29, 2020. The copyright holder for this preprint (which was not certified by peer review) is the author/funder. All rights reserved. No reuse allowed without permission.

Toda H, Kawasaki K, Sato S, Horie M, Nakahara K, Bepari AK, Sawahata H, Suzuki T, Okado H, Takebayashi H, Hasegawa I. 2018. Locally induced neuronal synchrony precisely propagates to specific cortical areas without rhythm distortion. *Sci Rep* **8**: 7678. doi:10.1038/s41598-018-26054-8

van Atteveldt N, Murray MM, Thut G, Schroeder CE. 2014. Multisensory integration: Flexible use of general operations. *Neuron* **81**:1240–1253. doi:10.1016/j.neuron.2014.02.044

van den Brink RL, Nieuwenhuis S, Donner TH. 2018. Amplification and suppression of distinct brainwide activity patterns by catecholamines. *J Neurosci* **38**: 7476–7491. doi:10.1523/JNEUROSCI.0514-18.2018

Varela F, Lachaux JP, Rodriguez E, Martinerie J. 2001. The brainweb: Phase synchronization and large-scale integration. *Nat Rev Neurosci* **2**:229–239. doi:10.1038/35067550

Wang P, Goeschl F, Friese U, Koenig P, Engel AK. 2018. Long-range functional coupling predicts performance: Oscillatory EEG networks in multisensory processing. *bioRxiv* 014423. doi: 10.1101/014423

Womelsdorf T, Fries P, Mitra PP, Desimone R. 2006. Gamma-band synchronization in visual cortex predicts speed of change detection. *Nature* **439**: 733–736. doi:10.1038/nature04258

Womelsdorf T, Fries P. 2007. The role of neuronal synchronization in selective attention. *Curr Opin Neurobiol* **17**:154–160. doi:10.1016/j.conb.2007.02.002

Womelsdorf T, Schoffelen J-M, Oostenveld R, Singer W, Desimone R, Engel AK, Fries P. 2007. Modulation of neuronal interactions through neuronal synchronization. *Science* **316**: 1609–1612. doi:10.1126/science.1139597

Zohary E, Shadlen MN, Newsome WT. 1994. Correlated neuronal discharge rate and its implications for psychophysical performance. *Nature* **370**:140. doi:10.1038/370140a0

bioRxiv preprint doi: https://doi.org/10.1101/579938; this version posted June 29, 2020. The copyright holder for this preprint (which was not certified by peer review) is the author/funder. All rights reserved. No reuse allowed without permission.

Tables

Table 1. Statistics for frequency resolved power analysis for hit and miss trials. The table shows *p*-values for all *t*-tests within frequency bands, trial outcome, and across all time points of interest; *italics* indicate significant comparisons ($p<0.001$; FDR corrected).

Frequency	Theta	Alpha	Beta	Gamma	High-Gamma
	Baseline vs. stimulus onset window				
Hit vs. hit	0.22	0.26	0.44	*>0.001*	0.053
Miss vs. miss	0.23	0.54	0.99	*>0.001*	*>0.001*
	Stimulus onset vs. response onset window				
Hit vs. hit	0.03	0.18	0.08	*>0.001*	*>0.001*
Miss vs. miss	0.21	0.62	0.53	0.08	*>0.001*
	Response onset window vs. baseline				
Hit vs. hit	0.10	0.46	0.98	0.01	*>0.001*
Miss vs. miss	0.25	0.58	0.79	*>0.001*	*>0.001*

Table 2. Statistics for frequency resolved functional connectivity analysis for all time points of interest for hit and miss trials. The table shows *p*-values for all *t*-tests within frequency bands, trial outcome and across all time points of interest; *italics* indicate significant contrasts (FDR corrected).

Frequency	Theta	Alpha	Beta	Gamma	High-Gamma
	Baseline vs. stimulus onset window				
Hit vs. hit	0.12	*<0.001*	*<0.001*	*<0.001*	*<0.001*
Miss vs. miss	0.75	*<0.001*	*<0.001*	*<0.001*	*<0.001*
	Stimulus onset vs. response onset window				
Hit vs. hit	0.03	*<0.001*	0.36	*<0.001*	*<0.001*
Miss vs. miss	0.79	0.07	0.67	0.17	*<0.001*
	Response onset window vs. baseline				
Hit vs. hit	*<0.001*	0.02	0.003	*<0.001*	*<0.001*
Miss vs. miss	0.84	*<0.001*	*<0.001*	*<0.001*	*<0.001*

bioRxiv preprint doi: https://doi.org/10.1101/579938; this version posted June 29, 2020. The copyright holder for this preprint (which was not certified by peer review) is the author/funder. All rights reserved. No reuse allowed without permission.

838 # Captions to figures

839 **Figure 1. Experimental setup and lateralized detection task.** (A) Schematic of the experimental
840 setup in a top view: a) LCD-screen, b) speakers, c) three light-barrier-waterspout combinations (left,
841 center, right; the red dot indicates a broken light-beam), d) pedestal. (B) Sequence of events in a single
842 trial: (I) inter-trial window, (II) baseline window, (III) delay window, (IV) stimulus window, and (V)
843 response window. The three circles below each frame represent the state of the light-barriers (white =
844 unbroken, red = broken). The center of the screen displays a static circular random noise pattern.
845
846 **Figure 2. ECoG recordings from the ferret brain.** (A) Lateral view of the left hemisphere. Lines
847 depict sulci in the posterior part of the hemisphere. (B) Anatomical organization of the posterior part
848 of the ferret brain (adopted from Bizley et al., 2007). (C) Schematic of the implanted ECoG (contact
849 spacing: 1.5mm; ø: 250µm). (D) In-situ picture of the ECoG array over the left posterior hemisphere
850 during implantation. Abbreviations: LS, lateral sulcus; SSS, suprasylvian sulcus; S2, secondary
851 somatosensory cortex; PPr/c, rostral/caudal posterior parietal cortex; 17, 18, 19, 20, 21, early and
852 higher-order visual cortex; SSY, suprasylvian field; A1, primary auditory cortex; AAF, anterior
853 auditory field; ADF, anterior dorsal field; PPF, posterior pseudosylvian field; PSF, posterior
854 suprasylvian field.
855
856 **Figure 3. Trial selection for electrophysiological analysis and corresponding RTs.** (A) Example
857 data for task performance from one ferret. The plot shows psychometric functions for the uni- and
858 bimodal condition. Stimulus response function fitted to performance data for the eight different
859 stimulus intensities for the unimodal auditory condition (A) and the condition where the variable
860 auditory stimulus was accompanied by a visual stimulus of constant contrast (Av). The dot diameter
861 indicates the number of trials at a given stimulus intensity. The green ellipse indicates the stimulus
862 intensity range around 75% performance from which trials were selected for subsequent analysis. The
863 unmasked parts of the graphs indicate the range of the actually tested stimulus amplitudes. (B) Data
864 from the same animal as shown in A for the unimodal visual condition (V) and the condition where
865 the variable visual stimulus was accompanied by an auditory stimulus of constant intensity (Va). (C)

bioRxiv preprint doi: https://doi.org/10.1101/579938; this version posted June 29, 2020. The copyright holder for this preprint (which was not certified by peer review) is the author/funder. All rights reserved. No reuse allowed without permission.

Grand average of reaction times (RT; sec. ± standard deviation) for the four different conditions for the selected trials. Asterisks indicate significant differences between modalities or pooled data from bimodal (Va and Av) and unimodal (A and V) stimulus pairs (brackets).

Figure 4. Spectral power analysis of pooled hit and miss trials. (A) Grand average power spectra for all hit (green) and miss (red) trials±standard error of the mean (SEM). For the baseline window absolute power is shown. Note that for the windows around stimulus and response onset, the spectral change relative to the baseline window is displayed. Asterisks indicate significant differences between hits and misses within the specified frequency band (FDR corrected). Labels indicate theta, alpha, beta, gamma and high-gamma band, respectively. (B) Time-frequency representation of power in the three analysis time windows, expressed as change relative to baseline before trial onset for all hit and miss trials. The vertical line represents trial, stimulus and response onset, respectively.

Figure 5. Grand average of functional connectivity for hit and miss trials. (A) Grand average phase locking value (PLV) for all hit (green) and miss (red) trials for the analysis time windows (baseline, stimulus and response onset). (B) Differences between hits and misses for the three analysis windows and changes of PLV around stimulus and response onset, expressed as changes relative to the baseline window. Asterisks indicate significant differences between hits and misses within the specified frequency band (FDR corrected). Labels in A denote theta, alpha, beta, gamma and high-gamma band, respectively.

Figure 6. Matrices of functional connectivity across anatomical areas. Cells show population average phase locking values (PLV) for the different frequency bands, expressed as d' for hits vs. misses, for all analysis time windows. Abbreviations as in Fig. 2.

Figure 7. Eigenconnectivity (EC) of hit and miss trials for the baseline window. Depicted are EC networks for beta and gamma of the first two PCs, which together explain 42% and 32% of the variance in the PCA for hits and misses, respectively. Green and red arrows represent hit and miss

bioRxiv preprint doi: https://doi.org/10.1101/579938; this version posted June 29, 2020. The copyright holder for this preprint (which was not certified by peer review) is the author/funder. All rights reserved. No reuse allowed without permission.

894 networks, respectively. Thick solid lines indicate the upper 10%, and thin dashed lines the lowest 10%
895 of connections in the eigenconnectivity distribution. Arrowheads indicate the direction of information
896 flow extracted by PSI. Colored circle segments represent the three functional systems (visual =
897 magenta; parietal = blue; auditory = orange). Note that EC matrices for the first 6 PCs with all
898 connection are shown in Suppl. Fig. 4. Abbreviations as in Fig. 2.
899
900 **Figure 8. Comparison of long-range (between-systems) and short-range (within-system)**
901 **functional connectivity.** (Left) Cortical regions were grouped into visual (magenta), parietal (blue), or
902 auditory (orange) systems. PLV was averaged for all pairs of regions that were located within the
903 same system (grey arrows) and pairs between systems (red arrows). Subsequently, d' was calculated
904 for hit and miss trial PLVs. (Right) Differences of between-region and within-region PLV (expressed
905 as d') are plotted as a function of carrier frequencies. Large values indicate higher between-system
906 PLV during hit compare to miss trials. Symbols indicate significant differences between baseline and
907 stimulus onset (*), baseline and response onset (o), and stimulus onset to response onset (+),
908 respectively.

bioRxiv preprint doi: https://doi.org/10.1101/579938; this version posted June 29, 2020. The copyright holder for this preprint (which was not certified by peer review) is the author/funder. All rights reserved. No reuse allowed without permission.

Supplements

Supplementary Table 1. One-way ANOVA results between the four conditions (Av, Va, A and V) as main factor for the data shown in Supplementary Figure 1.

Frequency	Theta	Alpha	Beta	Gamma	High-Gamma
Time					
Baseline	$F(3, 44) = 0.02$, $p>0.05$	$F(3, 76) = 0.03$, $p>0.05$	$F(3, 60) = 0.01$, $p>0.05$	$F(3, 412) = 0.02$, $p>0.05$	$F(3, 652) = 0.09$, $p>0.05$
Stimulus onset	$F(3, 44) = 0.03$, $p>0.05$	$F(3, 76) = 0.01$, $p>0.05$	$F(3, 60) = 0$, $p>0.05$	$F(3, 412) = 0.4$, $p>0.05$	$F(3, 652) = 0.06$, $p>0.05$
Response onset	$F(3, 44) = 0.02$, $p>0.05$	$F(3, 76) = 0.03$, $p>0.05$	$F(3, 60) = 0.02$, $p>0.05$	$F(3, 412) = 0.05$, $p>0.05$	$F(3, 652) = 0.07$, $p>0.05$

Supplementary Table 2. *p*-values of the post hoc *t*-test results for data shown in Supplementary Figure 3 for the baseline analysis window; *italics* indicate significant contrasts (Bonferroni corrected).

Frequency	Theta	Alpha	Beta	Gamma	High-Gamma
A → V	>0.05	*0.004*	*0.035*	*<0.001*	*<0.001*
A → Av	>0.05	>0.05	>0.05	>0.05	>0.05
A → Va	>0.05	>0.05	>0.05	*<0.001*	*<0.001*
V → Av	>0.05	>0.05	>0.05	*<0.001*	*<0.001*
V →Va	>0.05	>0.05	>0.05	*0.038*	*0.003*
Av → Va	>0.05	>0.05	>0.05	*<0.001*	*<0.001*

Supplementary Table 3. *p*-values of the post hoc *t*-test results for data shown in Supplementary Figure 3 for the stimulus onset analysis window; *italics* indicate significant contrasts (Bonferroni corrected).

Frequency	Theta	Alpha	Beta	Gamma	High-Gamma
A → V	>0.05	*0.022*	*0.025*	*<0.001*	*<0.001*
A → Av	>0.05	>0.05	>0.05	>0.05	>0.05
A → Va	>0.05	>0.05	>0.05	*<0.001*	*<0.001*
V → Av	>0.05	>0.05	>0.05	*<0.001*	*<0.001*
V →Va	>0.05	>0.05	>0.05	>0.05	*0.002*
Av → Va	>0.05	>0.05	>0.05	*<0.001*	*<0.001*

bioRxiv preprint doi: https://doi.org/10.1101/579938; this version posted June 29, 2020. The copyright holder for this preprint (which was not certified by peer review) is the author/funder. All rights reserved. No reuse allowed without permission.

Supplementary Table 4. *p*-values of the post hoc *t*-test results for data shown in Supplementary Figure 3 for the response onset analysis window; *italics* indicate significant contrasts (Bonferroni corrected).

Frequency	Theta	Alpha	Beta	Gamma	High-Gamma
A → V	>0.05	*0.035*	*0.02*	*<0.001*	*<0.001*
A → Av	>0.05	>0.05	>0.05	>0.05	>0.05
A → Va	>0.05	>0.05	>0.05	*<0.001*	*<0.001*
V → Av	>0.05	>0.05	>0.05	*<0.001*	*<0.001*
V →Va	>0.05	>0.05	>0.05	>0.05	*0.005*
Av → Va	>0.05	>0.05	>0.05	*0.002*	*<0.001*

Supplementary Table 5. Two-way ANOVA results with System (within auditory; within visual; within parietal; between visual and auditory; between visual and parietal: between auditory and parietal) and Time (Baseline, stimulus and response onset) as main factors for the data shown in Supplementary Figure 4.

Frequency	Theta	Alpha	Beta	Gamma	High-Gamma	Broadband
ANOVA						
System	$F(5, 375) = 17.69$, $p<0.001$	$F(5, 375) = 30.55$, $p<0.001$	$F(5, 375) = 17.31$, $p<0.001$	$F(5, 375) = 18.9$, $p<0.001$	$F(5, 375) = 15.45$, $p<0.001$	$F(5, 375) = 18.85$, $p<0.001$
Time	$F(2, 375) = 12.17$, $p<0.001$	$F(2, 375) = 8.33$, $p<0.001$	$F(2, 375) = 5.4$, $p=0.005$	$F(2, 375) = 7.15$, $p<0.001$	$F(2, 375) = 6.79$, $p=0.001$	$F(2, 375) = 12.23$, $p<0.001$
Interaction	$F(10, 375) = 0.88$, $p>0.05$	$F(10, 375) = 0.55$, $p>0.05$	$F(10, 375) = 0.6$, $p>0.05$	$F(10, 375) = 0.35$, $p>0.05$	$F(10, 375) = 0.44$, $p>0.05$	$F(10, 375) = 0.51$, $p>0.05$

Supplementary Table 6. ANOVA and post hoc *t*-test (*p*-values) results for data shown in Supplementary Figure 5 for the auditory modality; *italics* indicate significant contrasts (Bonferroni corrected). Abbreviations: BL = Baseline; SO = Stimulus-onset; RO = Response-onset.

Frequency	Theta	Alpha	Beta	Gamma	High-Gamma
ANOVA	$F(2, 6) = 0.23$, $p>0.05$	$F(2, 12) = 7.32$, $p=0.008$	$F(2, 9) = 8.03$, $p=0.01$	$F(2, 75) = 7.45$, $p=0.001$	$F(2, 120) = 5.01$, $p=0.008$
Post hoc *t*-test					
BL → SO	>0.05	0.04	0.01	*0.004*	0.01
SO → RO	>0.05	>0.05	>0.05	*0.004*	>0.05
BL → RO	>0.05	0.01	>0.05	>0.05	>0.05

bioRxiv preprint doi: https://doi.org/10.1101/579938; this version posted June 29, 2020. The copyright holder for this preprint (which was not certified by peer review) is the author/funder. All rights reserved. No reuse allowed without permission.

Supplementary Table 7. ANOVA and post hoc *t*-test (*p*-values) results for data shown in Supplementary Figure 5 for the visual modality; *italics* indicate significant contrasts (Bonferroni corrected). Abbreviations: BL = Baseline; SO = Stimulus-onset; RO = Response-onset.

Frequency	Theta	Alpha	Beta	Gamma	High-Gamma
ANOVA	$F(2, 6) = 4.21$, $p>0.05$	$F(2, 12) = 8.53$, $p=0.005$	$F(2, 9) = 5.33$, $p=0.03$	$F(2, 75) = 10.62$, $p<0.001$	$F(2, 120) = 9.63$, $p<0.001$
Post hoc *t*-test					
BL → SO	>0.05	>0.05	>0.05	*0.001*	*0.001*
SO → RO	>0.05	>0.05	>0.05	>0.05	*0.002*
BL → RO	>0.05	*0.004*	0.04	>0.05	>0.05

Supplementary Table 8. ANOVA and post hoc *t*-test (*p*-values) results for data shown in Supplementary Figure 5 for the auditory stimulation accompanied by a constant visual stimulus (Av); *italics* indicate significant contrasts (Bonferroni corrected). Abbreviations: BL = Baseline; SO = Stimulus-onset; RO = Response-onset.

Frequency	Theta	Alpha	Beta	Gamma	High-Gamma
ANOVA	$F(2, 6) = 1.65$, $p>0.05$	$F(2, 12) = 12.14$, $p=0.001$	$F(2, 9) = 5.25$, $p=0.031$	$F(2, 75) = 10.37$, $p<0.001$	$F(2, 120) = 17.96$, $p<0.001$
Post hoc *t*-test					
BL → SO	>0.05	0.02	0.04	*0.001*	*<0.001*
SO → RO	>0.05	>0.05	>0.05	>0.05	*0.006*
BL → RO	>0.05	*0.001*	>0.05	0.01	0.02

Supplementary Table 9. ANOVA and post hoc *t*-test (*p*-values) results for the data shown in Supplementary Figure 5 for the visual stimulation accompanied by a constant auditory stimulus (Va); *italics* indicate significant contrasts (Bonferroni corrected). *Abbreviations:* BL = Baseline; SO = Stimulus-onset; RO = Response-onset.

Frequency	Theta	Alpha	Beta	Gamma	High-Gamma
ANOVA	$F(2, 6) = 5.09$, $p>0.05$	$F(2, 12) = 6.66$, $p=0.011$	$F(2, 9) = 4.07$, $p>0.05$	$F(2, 75) = 5.88$, $p=0.004$	$F(2, 120) = 11.12$, $p<0.001$
Post hoc *t*-test					
BL → SO	>0.05	>0.05	>0.05	0.04	*<0.001*
SO → RO	>0.05	>0.05	>0.05	>0.05	0.03
BL → RO	>0.05	0.01	>0.05	>0.05	>0.05

bioRxiv preprint doi: https://doi.org/10.1101/579938; this version posted June 29, 2020. The copyright holder for this preprint (which was not certified by peer review) is the author/funder. All rights reserved. No reuse allowed without permission.

948 **Supplementary Figure 1. Spectral power for uni- and bimodal stimulation conditions.** Grand
949 average power spectra for baseline, stimulus and response onset for all hit trials (green), all miss trials
950 (red) and for the hit trials of each stimulus condition (Av: blue; Va: yellow; A: orange; V: purple). For
951 the baseline window absolute power is shown. Note that for the windows centered around stimulus
952 and response onset, the spectral change relative to the baseline window is displayed. For ANOVA
953 results, see Supplementary Table 1.
954
955 **Supplementary Figure 2. Frequency specific power topographies for all analysis time windows**.
956 Topographic representation of power for all frequency bands and analysis time windows, expressed as
957 d' for the difference between hits and misses. High values indicate dominance during hit compare to
958 miss trials. Negative values indicate increased power during the miss compare to hit trials.
959 Abbreviations: LS, lateral sulcus; SSS, suprasylvian sulcus.
960
961 **Supplementary Figure 3. Grand average functional connectivity for uni- and bimodal**
962 **stimulation conditions.** Grand average phase locking value (PLV) for all analysis time windows
963 (baseline, stimulus and response onset) for all hit trials (green), all miss trials (red) and for the hit trials
964 of each stimulus condition (Av: blue; Va: yellow; A: orange; V: purple).
965
966 **Supplementary Figure 4. Eigenconnectivity (EC) matrices of principal component (PC) 1-6 for**
967 **the baseline time window**. Population averaged EC matrices, displayed are the upper and lower 10%
968 of each EC distribution for all frequency bands of interest. The color code depicts the eigenvalues of
969 the thresholded connections. The upper right half of each matrix corresponds to miss trials (red
970 contour) and the lower left part to hit trials (green contour). Abbreviations as in Fig. 2.

bioRxiv preprint doi: https://doi.org/10.1101/579938; this version posted June 29, 2020. The copyright holder for this preprint (which was not certified by peer review) is the author/funder. All rights reserved. No reuse allowed without permission.

Supplementary Figure 5. Within- and between system functional connectivity for all frequencies and analysis time windows. Cortical regions were grouped into visual (magenta), parietal (blue), or auditory (orange) systems. PLV was averaged for all pairs of regions that were located within the same system (grey arrows) and pairs between systems (red arrows). Bar plots display the sensitivity index (d') for difference between hit and miss trial PLV for the theta, alpha, beta, gamma, high-gamma frequency bands, as well as for broadband (BB) data averaged across all frequency bands. Panels show data for within system PLV (left) and between system PLV (right) for all analysis time windows. Lines between bars indicate significant differences. For ANOVA results, see Supplementary Table 5.

Supplementary Figure 6. Modality specific comparison of long-range (between-systems) and short-range (within-system) functional connectivity. (Top) Cortical regions were grouped into visual (magenta), parietal (blue), or auditory (orange) systems. PLV was averaged for all pairs of regions that were located within the same system (grey arrows) and pairs between systems (red arrows). Subsequently, d' was calculated for hit and miss trial PLVs. (Bottom) Plots shows the differences of between-region and within-region PLV (d') as a function of carrier frequencies for each stimulation condition (Top left: A; top right: V; bottom left: Av; bottom right: Va). Large values indicate higher between-system PLV during hit compare to miss trials. Symbols indicate significant differences between baseline and stimulus onset (*), baseline and response onset (o), and stimulus onset to response onset (+), respectively. For modality specific ANOVA and post hoc *t*-test results see Supplementary Tables 6-9.

bioRxiv preprint doi: https://doi.org/10.1101/579938; this version posted June 29, 2020. The copyright holder for this preprint (which was not certified by peer review) is the author/funder. All rights reserved. No reuse allowed without permission.

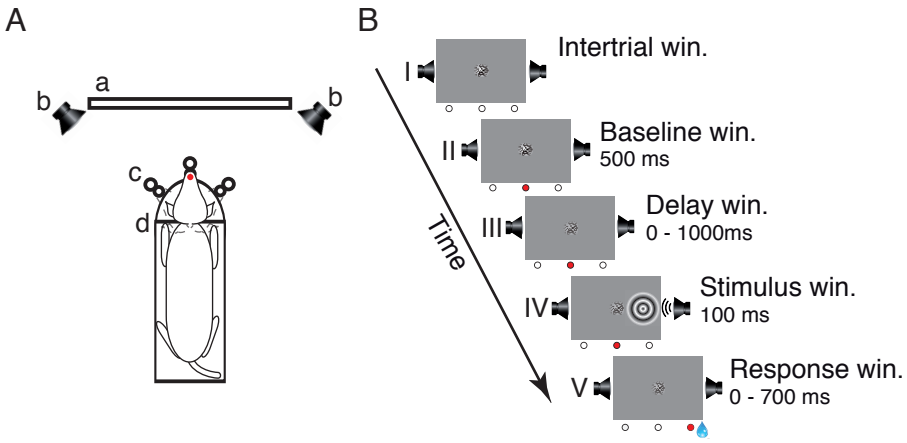

bioRxiv preprint doi: https://doi.org/10.1101/579938; this version posted June 29, 2020. The copyright holder for this preprint (which was not certified by peer review) is the author/funder. All rights reserved. No reuse allowed without permission.

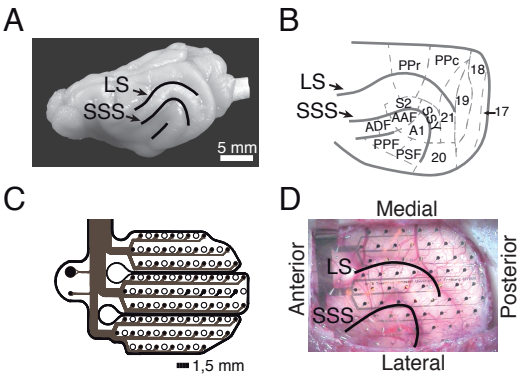

bioRxiv preprint doi: https://doi.org/10.1101/579938; this version posted June 29, 2020. The copyright holder for this preprint (which was not certified by peer review) is the author/funder. All rights reserved. No reuse allowed without permission.

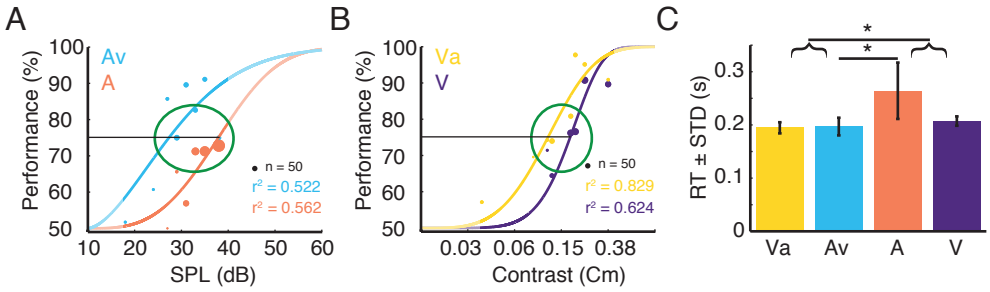

bioRxiv preprint doi: https://doi.org/10.1101/579938; this version posted June 29, 2020. The copyright holder for this preprint (which was not certified by peer review) is the author/funder. All rights reserved. No reuse allowed without permission.

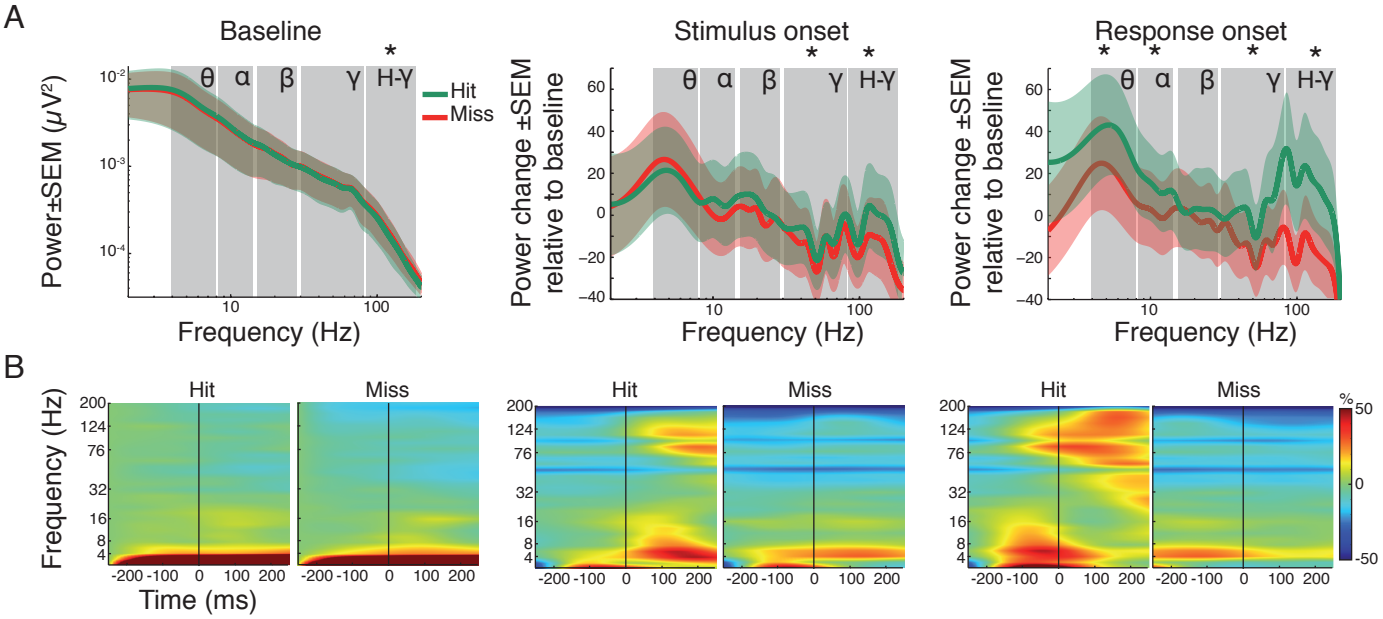

bioRxiv preprint doi: https://doi.org/10.1101/579938; this version posted June 29, 2020. The copyright holder for this preprint (which was not certified by peer review) is the author/funder. All rights reserved. No reuse allowed without permission.

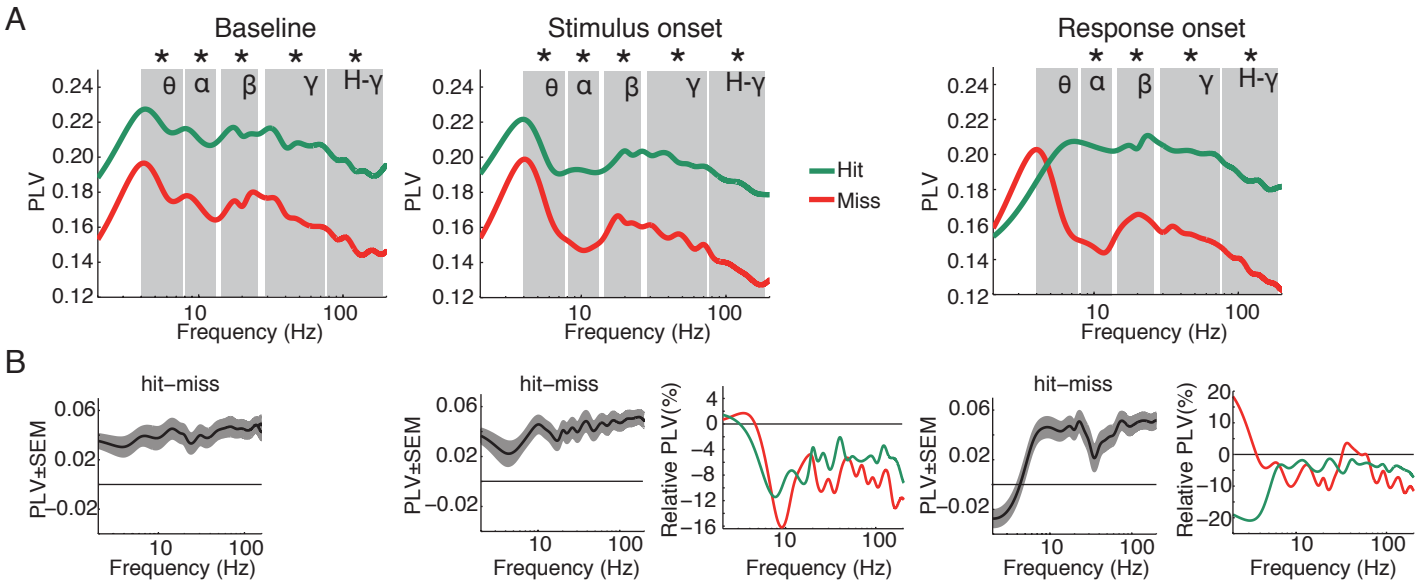

bioRxiv preprint doi: https://doi.org/10.1101/579938; this version posted June 29, 2020. The copyright holder for this preprint (which was not certified by peer review) is the author/funder. All rights reserved. No reuse allowed without permission.

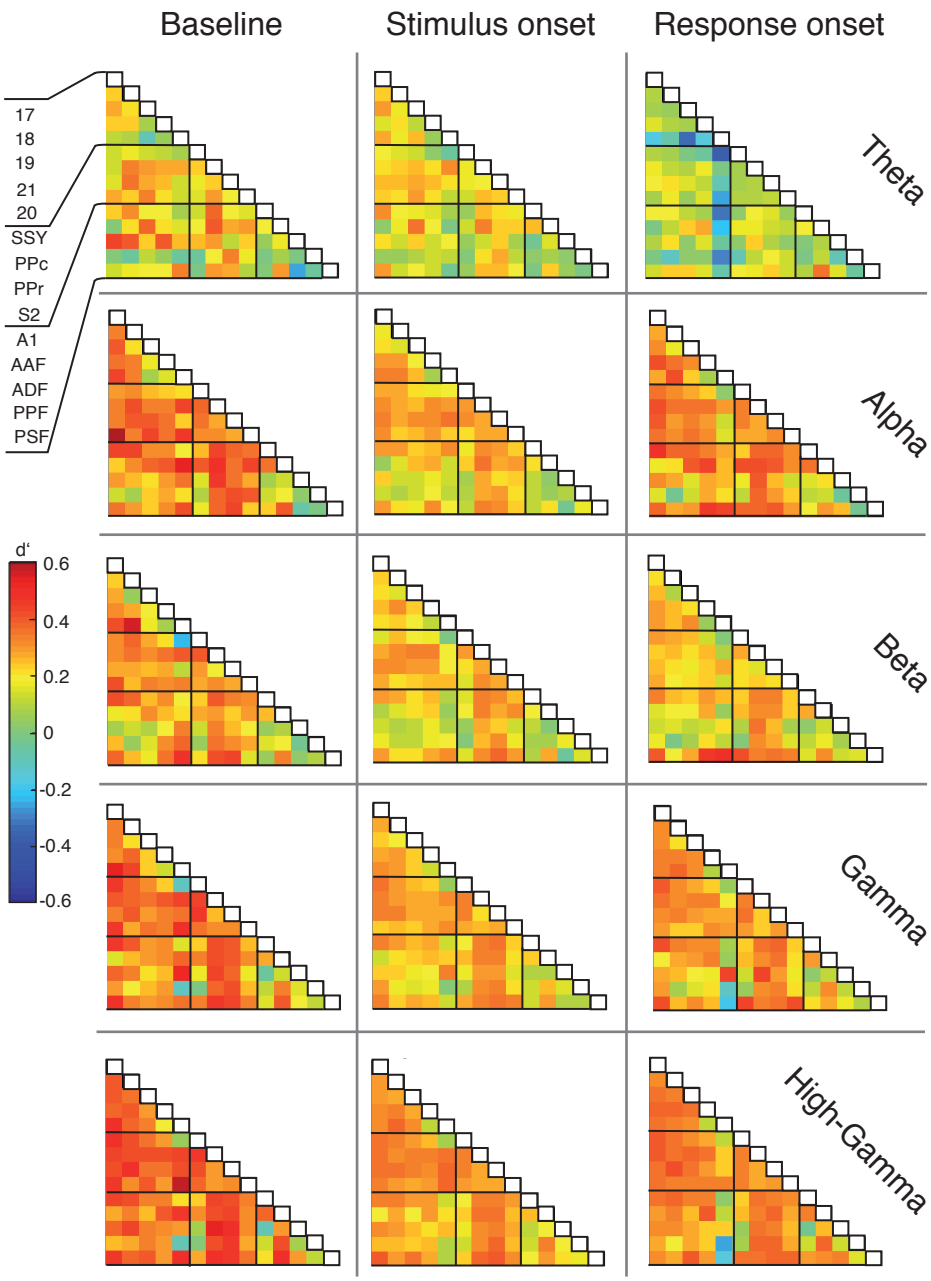

bioRxiv preprint doi: https://doi.org/10.1101/579938; this version posted June 29, 2020. The copyright holder for this preprint (which was not certified by peer review) is the author/funder. All rights reserved. No reuse allowed without permission.

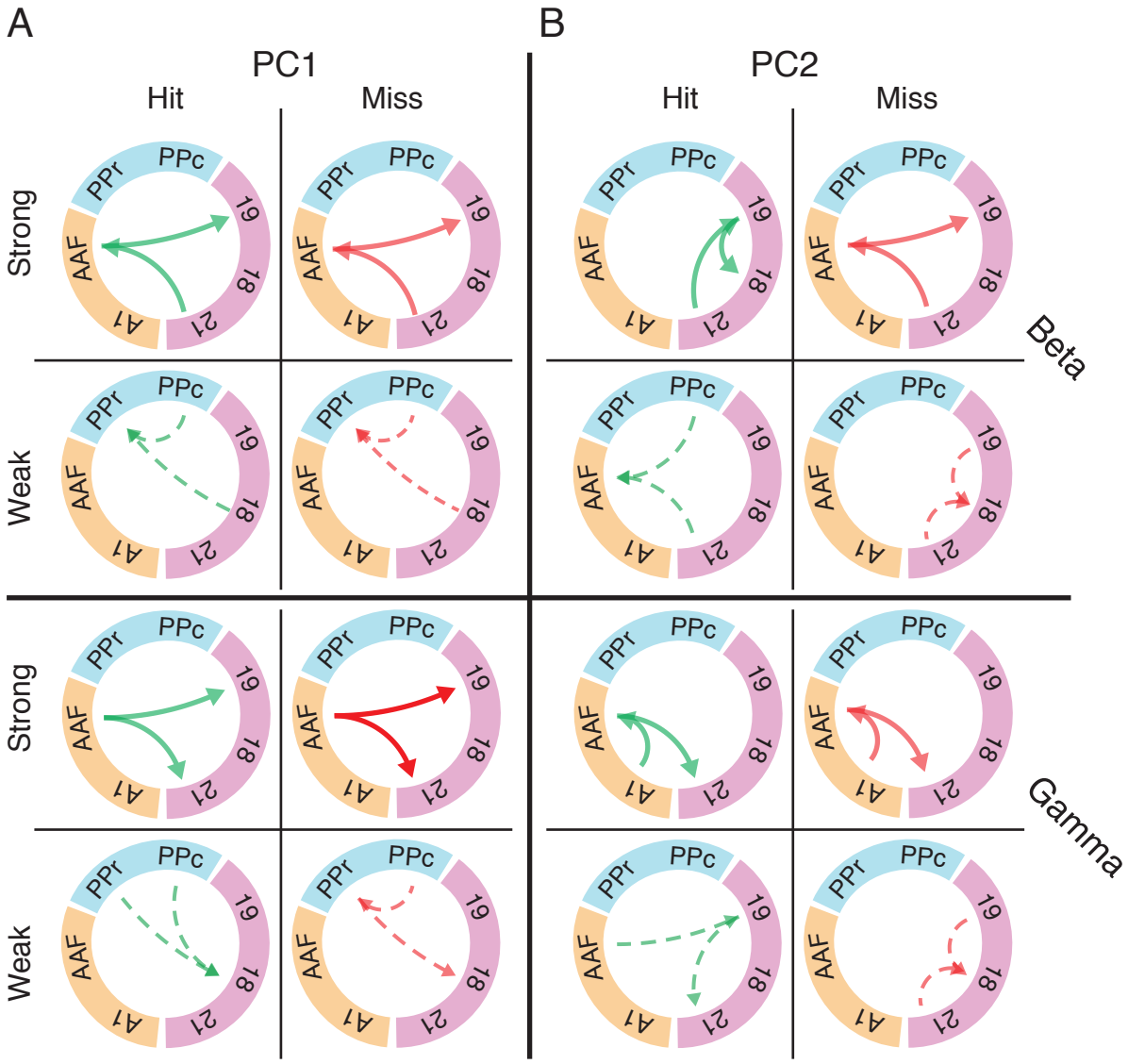

bioRxiv preprint doi: https://doi.org/10.1101/579938; this version posted June 29, 2020. The copyright holder for this preprint (which was not certified by peer review) is the author/funder. All rights reserved. No reuse allowed without permission.

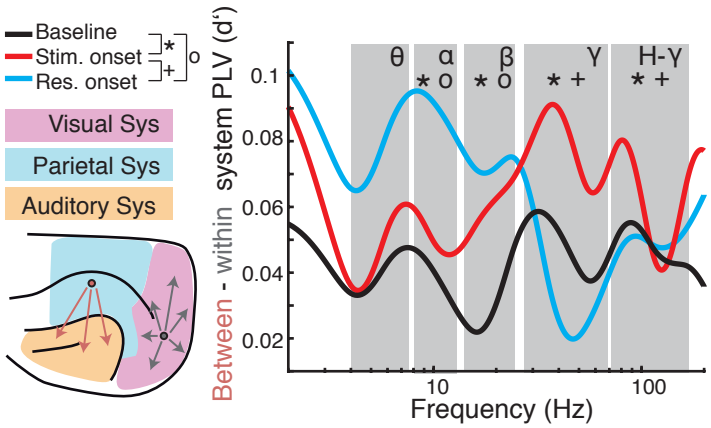

bioRxiv preprint doi: https://doi.org/10.1101/579938; this version posted June 29, 2020. The copyright holder for this preprint (which was not certified by peer review) is the author/funder. All rights reserved. No reuse allowed without permission.

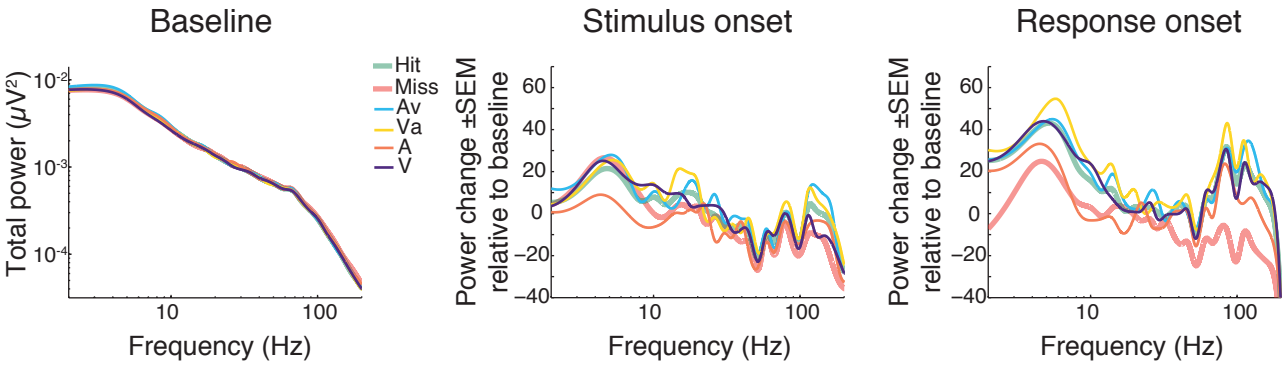

bioRxiv preprint doi: https://doi.org/10.1101/579938; this version posted June 29, 2020. The copyright holder for this preprint (which was not certified by peer review) is the author/funder. All rights reserved. No reuse allowed without permission.

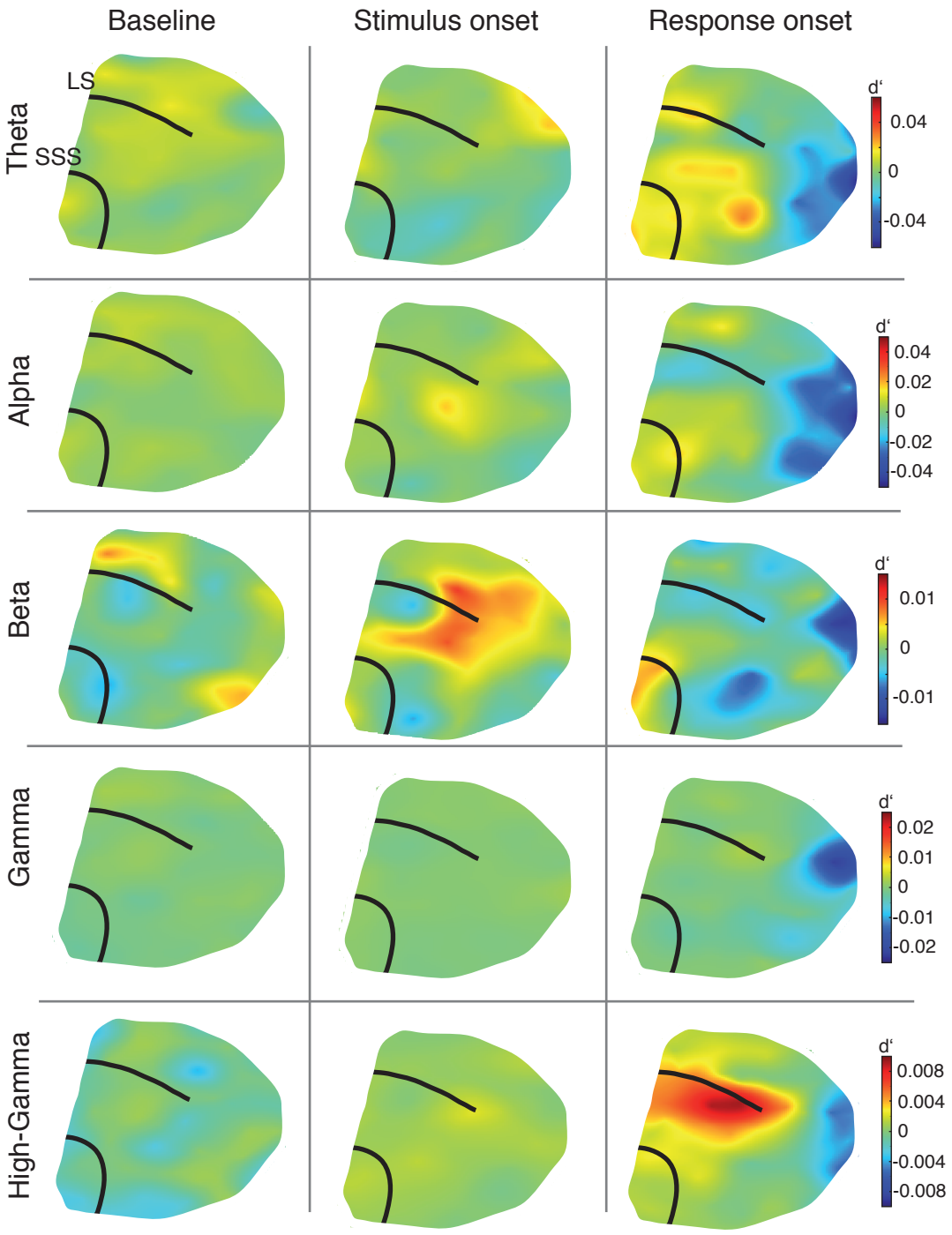

bioRxiv preprint doi: https://doi.org/10.1101/579938; this version posted June 29, 2020. The copyright holder for this preprint (which was not certified by peer review) is the author/funder. All rights reserved. No reuse allowed without permission.

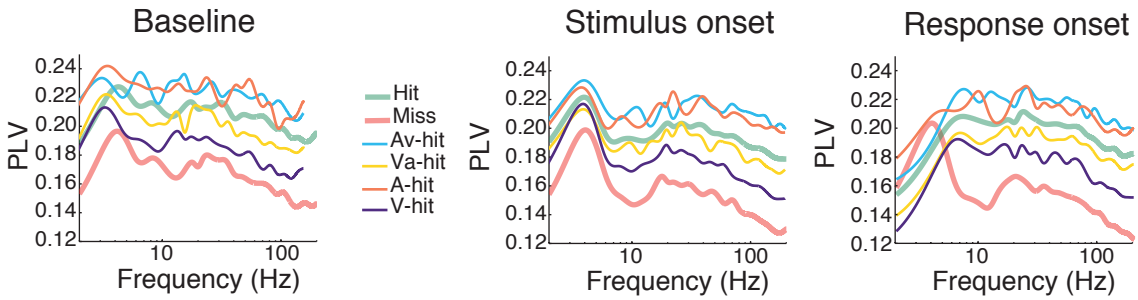

bioRxiv preprint doi: https://doi.org/10.1101/579938; this version posted June 29, 2020. The copyright holder for this preprint (which was not certified by peer review) is the author/funder. All rights reserved. No reuse allowed without permission.

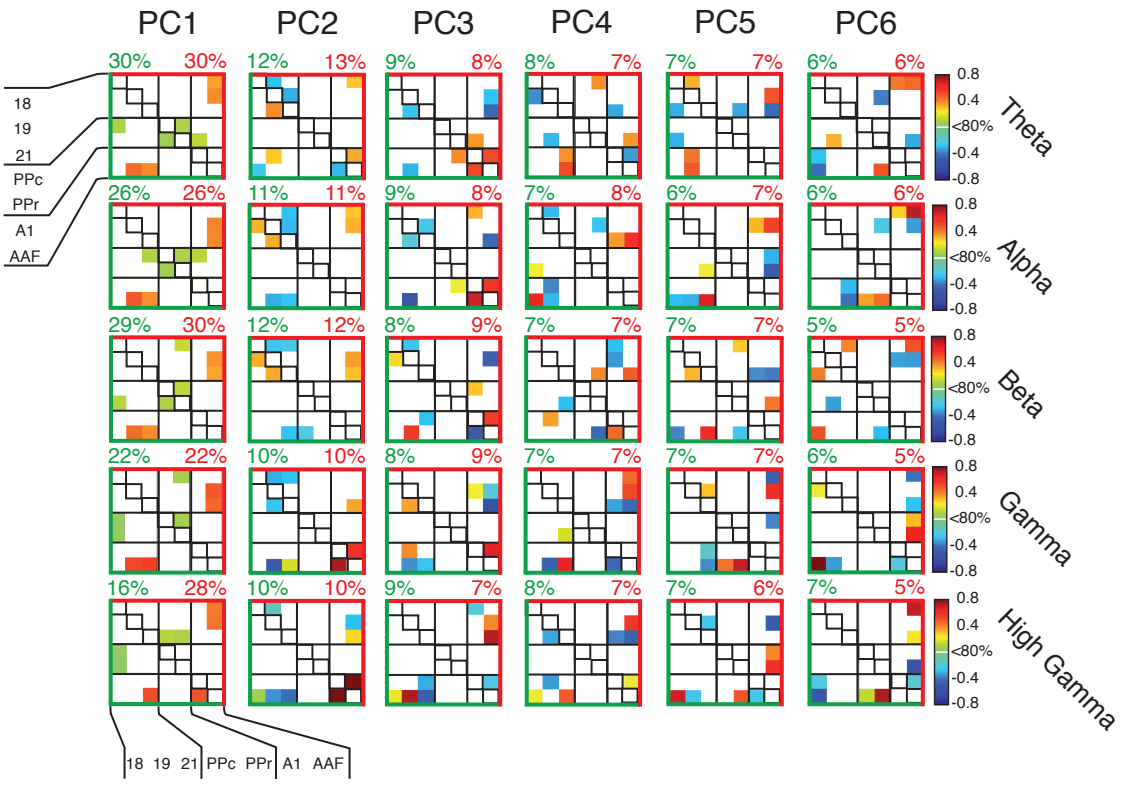

bioRxiv preprint doi: https://doi.org/10.1101/579938; this version posted June 29, 2020. The copyright holder for this preprint (which was not certified by peer review) is the author/funder. All rights reserved. No reuse allowed without permission.

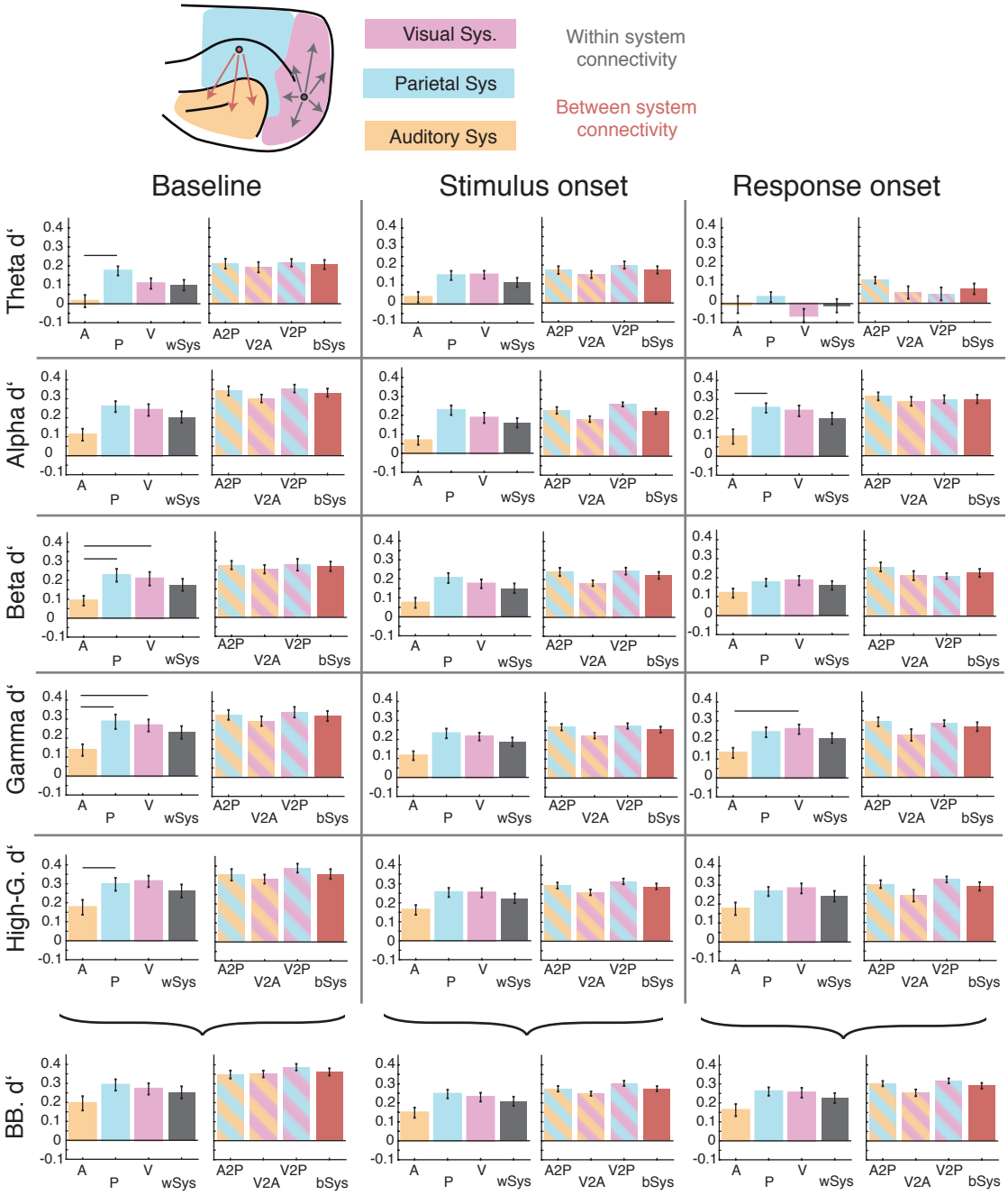
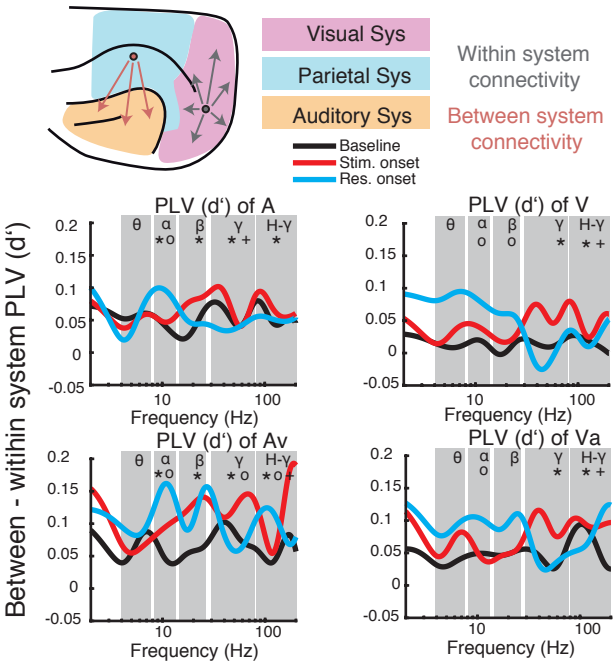
bioRxiv preprint doi: https://doi.org/10.1101/579938; this version posted June 29, 2020. The copyright holder for this preprint (which was not certified by peer review) is the author/funder. All rights reserved. No reuse allowed without permission.